Interferences: interferometers

Pascal Picart- Joëlle Surrel

14.04.2025

Table des matières

I.Présentation

Module :

Interferences and Diffraction

Auteur(s) :

Pascal PICART[1]&*Joëlle SURREL*[2] - ENSIM - Le Mans Université & IUT Saint-Étienne

Résumé :

The course proposes the description and analysis of interference devices based on amplitude division and wavefront division. The case study addresses different application aspects of interferometers: control of optical systems by Twyman-Green interferometry, Fourier transform spectroscopy, confocal scanning Fabry-Pérot spectrometry. The exercise part deals with the principle of a laser Doppler velocimeter.

Mots-clés :

interference, interferometers, Michelson interferometer, Fizeau interferometer, Twyman-Green interferometer, Sagnac interferometer, Fabry-Pérot interferometer, laser Doppler velocimetry

Pré-requis :

Complex numbers, waves, interference, Fourier transform

Objectif(s) pédagogique(s) :

Know the principles of the different wavefront division and amplitude division interferometers,

Know how to analyze the operation of an interferometer,

Understand the principles of controlling optical systems using interferometry, the principle of Fourier transform spectroscopy and confocal Fabry-Pérot interferometer spectrometry.

Plan du cours :

Conception & production :

Le Mans Université

Licence :

1 - pascal.picart@univ-lemans.fr
2 - joelle.surrel@univ-st-etienne.fr
3 - http://www.gnu.org/licenses/fdl.txt

II.Lesson

Interferometers are devices which create interferences between two or more waves. Interferometers are usually classified in two different groups. The first one deals with **wavefront-splitting** devices: a primary wavefront is divided in two **spatially different** beams that follow different paths before they are recombined and produce interferences. For example, the Young slits system configuration is part of this group. The second group deals with **amplitude-splitting** devices: a primary wavefront is divided in two spatially equal beams that follow different paths before they are recombined and produce interferences. The Michelson interferometer is part of this group.

The next paragraphs present the interferometers of both groups. The description of a Twyman-Green interferometer, the principle of Fourier transform spectroscopy and by Fabry-Perot interferometer will be developed in the case study. The principle of a laser Doppler velocimeter will be studied in the exercise part.

1. Wavefront-splitting interferometers

1.1. Young holes or slits

This device has been fully described in the first course dealing with interferences and called "**Interferences: fondamentals**". The reader is invited to use that lesson. We will just remind you that the system uses a primary source and two secondary sources that are either microscopic holes or thin slits (see figure 1) [1 [[1]]].

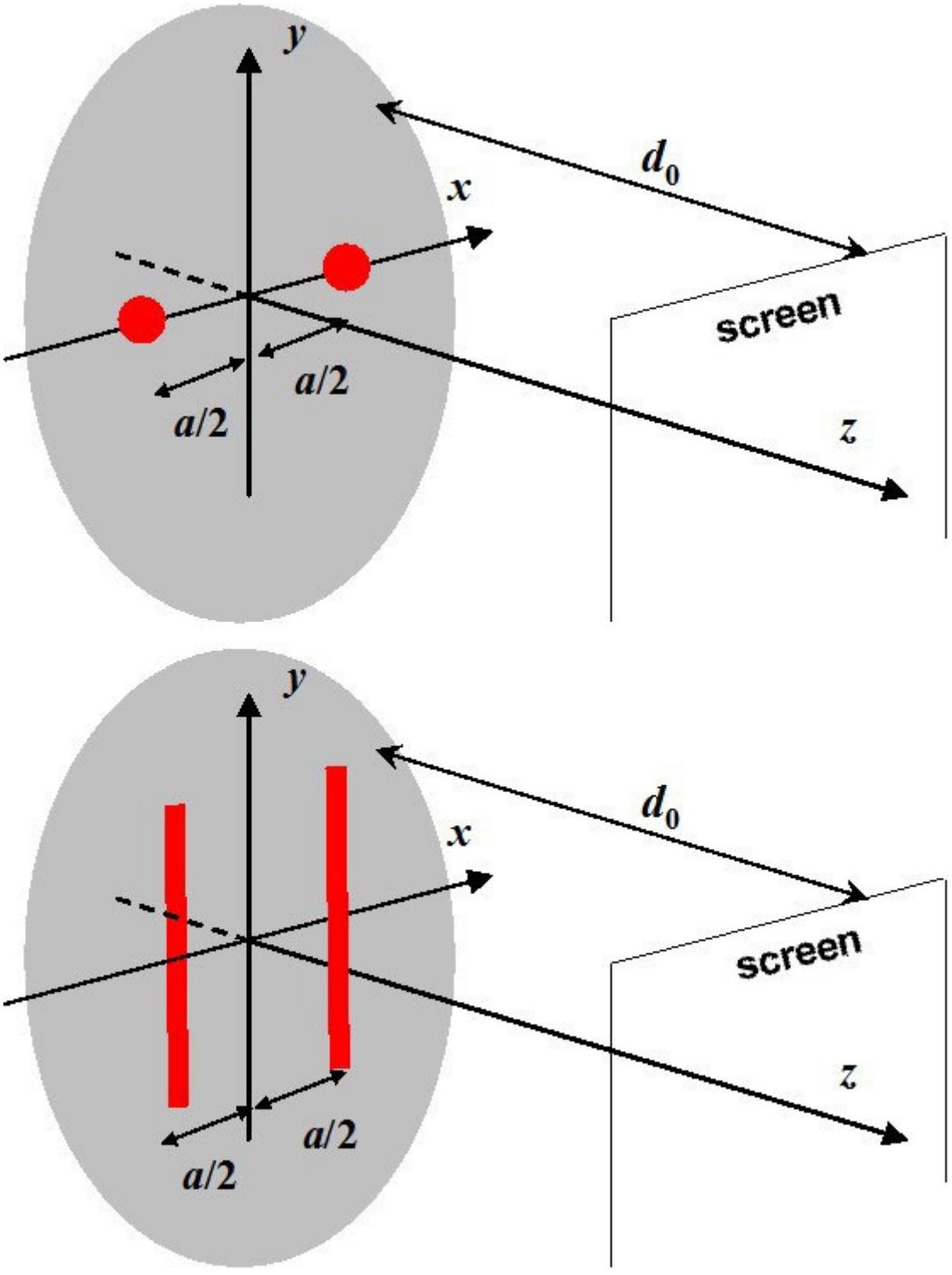

Remarque

The wavefront emitted by the primary source is divided into two distinct secondary wavefronts by the holes or slits that act as secondary sources. As the holes or slits are quite narrow, the light diffracts towards the screen so we can observe the interferences between both diffraction patterns of the secondary sources.

1.2. Fresnel mirrors

This device uses a primary source combined with two reflecting flat mirrors that make a slight angle α between their planes. Their source is located at the distance R on the mirror's edge. Each mirror gives a virtual image of the primary source and both images act as secondary sources. In the intersection area of both beams we can observe interferences. Figure 2 presents the Fresnel mirror interferometer.

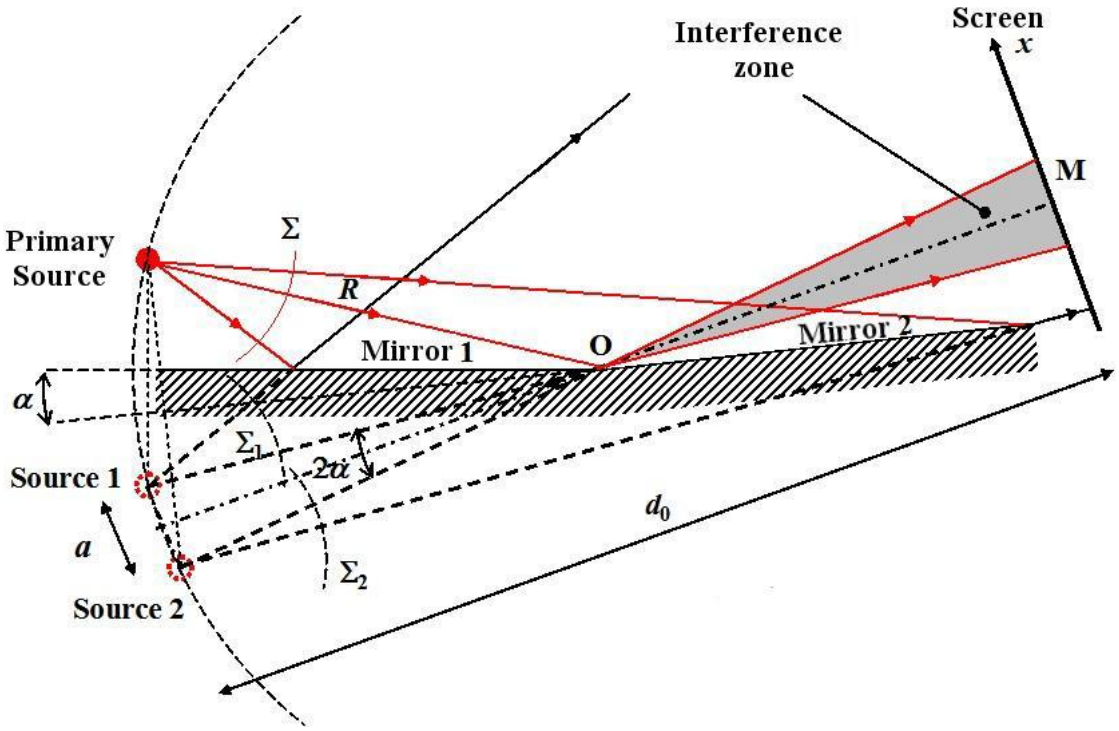

We demonstrate geometrically that the secondary sources are localized on a circle with center O and radius R. The screen is placed at the distance d_0 from the secondary sources, parallel to the plane of the source. The secondary sources are quantity a away . We recognize that we have to process the interferences between two spherical wavefronts emitted by both secondary sources. In all point $M(x, y, d_0)$, the interferences are written

$$I(x, y, d_0) = 2A^2\left(1+\cos\left(\varphi(x, y, d_0)\right)\right)$$

And in the case of the parabolic approximation where $d_0 \gg a$,

$$\varphi(x, y, d_0) \simeq \frac{2\pi}{\lambda}\frac{a\,x}{d_0}$$

As the angle α is small, we have the triangle (O, S_1, S_2):

$$2\alpha \simeq \frac{a}{R} \quad \text{soit} \quad a \simeq 2\alpha R$$

So comes :

$$\varphi(x, y, d_0) \simeq \frac{2\pi}{\lambda} \frac{2\alpha R x}{d_0}$$

And the interfringe is :

$$i = \frac{\lambda d_0}{2\alpha R}$$

Remarque

To define the fringes's geometric shape, we will determine the location of the points for which the phase is constant, which leads to $x = Cte$. The fringes are vertical, perpendicular to the figure plane, and regularly spaced from the interfringe i.

1.3. Lloyd Mirror

This device uses a primary source associated with a mirror and a screen placed perpendicularly to the mirror plane. Figure 3 represents the Lloyd mirror device.

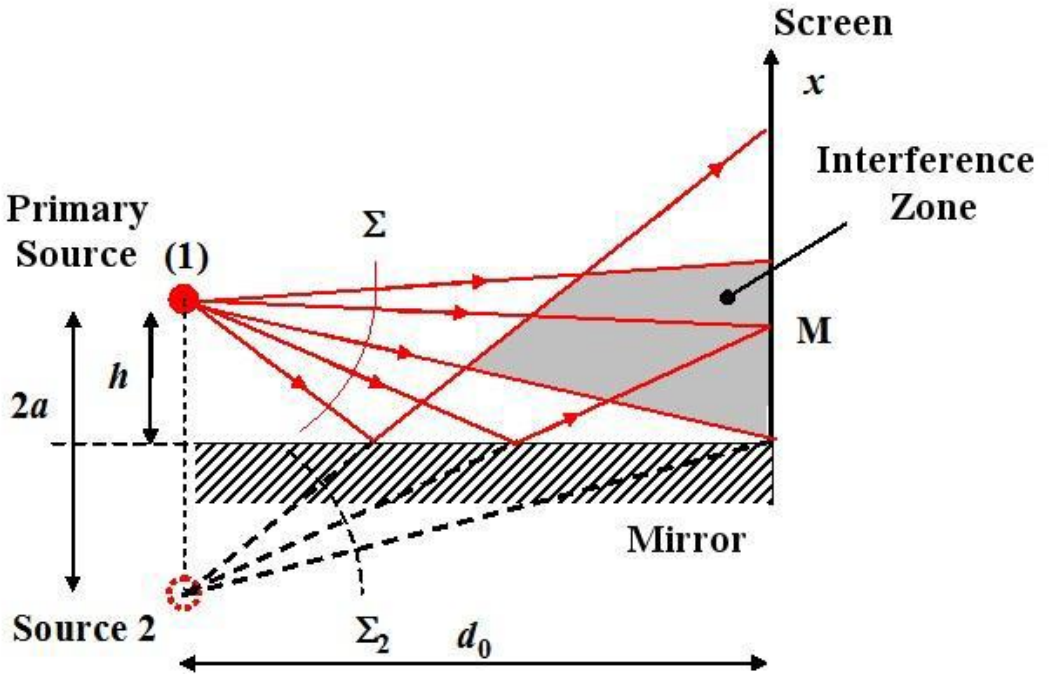

The secondary source, primary source image given by the mirror, is symmetrical to the mirror plane. So both sources are the primary source and its image through the mirror. As the primary source is located at the height h of the mirror plan, the distance between both sources is $a = 2h$. The screen is located at the distance d_0 from both sources, perpendicularly to the mirror plan. As before, we have to process the interferences between two spherical wavefronts emitted by two identical sources.

Remarque

If the mirror reflects 100% of the light, in all points $M(x, y, d_0)$, the interferences are written :

$$I(x, y, d_0) = 2A^2\left(1+\cos\left(\varphi(x, y, d_0)\right)\right)$$

And in the case where $d_0 \gg a$:

$$\varphi(x, y, d_0) \simeq \frac{2\pi}{\lambda}\frac{a\,x}{d_0}$$

And the interfringe is :

$$i = \frac{\lambda\, d_0}{2h}$$

To define the fringes geometrical shape, we seek the place of the points whose phase is constant, which leads to $x = Cte$. The fringes are vertical, perpendicular to the figure plane, and regularly spaced form the interfringe i.

1.4. Billet Bi-Lens

This device uses a primary source with a lens split into two half-lenses with respects to its diameter, and a screen placed perpendicularly to the bi-lens optical axis. Figure 4 represents the Billet Bi-Lens device.

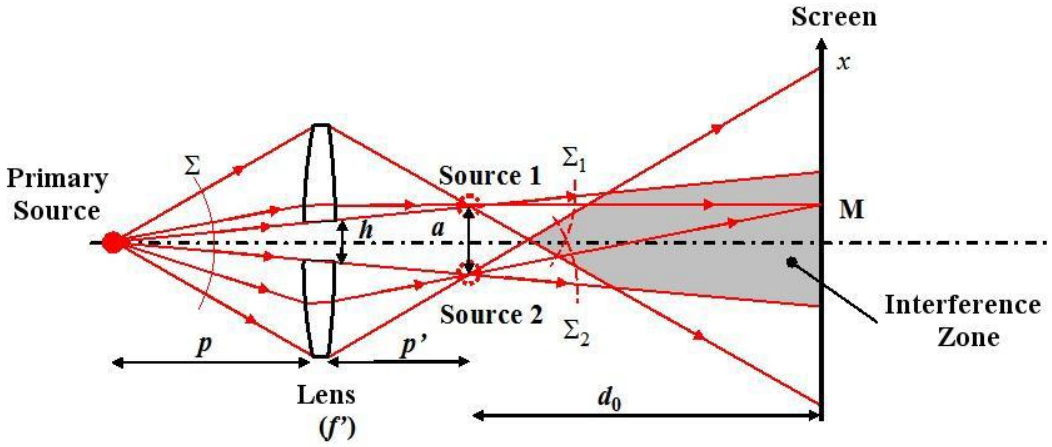

Each half-lens gives its own image of the primary source. Therefore each image constitutes a secondary source. The screen is placed at the distance d_0 from the secondary sources, namely at the distance $p' + d_0$ from the bi-lens. If the bi-lens is moved away from the quantity h and the primary source placed at the distance p, then the secondary sources are located at the distance p' such as:

$$p' = \frac{p\,f'}{p+f'}$$

And they are moved apart from the quantity a such as:

$$a = h\frac{p'}{p}$$

As before, we can observe that the interferences between two spherical wavefronts emitted by the same two amplitude sources and in all point $M(x, y, d_0)$, the interferences are written

$$I(x, y, d_0) = 2A^2\left(1+\cos\left(\varphi(x, y, d_0)\right)\right)$$

And in the case where $d_0 \gg a$:

$$\varphi(x, y, d_0) \simeq \frac{2\pi}{\lambda}\frac{a\,x}{d_0} = \frac{4\pi}{\lambda}\frac{h\,p'\,x}{p\,d_0}$$

And the interfringe is:

$$i = \frac{\lambda\, d_0\, p}{h\, p'}$$

Attention

The interfringe is constant following the direction x and the fringes are vertical, perpendicular to the figure plane.

2. Amplitude-splitting interferometers

For these devices, the source extension makes it possible to have more luminous devices than in the case of wavefront-splitting interferometers but the interferences fringes are localized.

2.1. Glass plate

The simplest wavefront-splitting interferometric system is given by a glass plate or a glass corner observed in reflection. This paragraph is strongly based on Chapter 6 of reference [1 [[1]]].

During the refraction on an air-glass type diopter, about 4% of the light energy is reflected. So the light reflected or transmitted can be the cause of an interference phenomenon. In this paragraph we will only deal with the interferences by reflection, as the transmission case is similar. An extended and monochromatic source located in the air illuminates a plate with parallel sides of index n, of thickness e (figure 5) put down on a third medium of index n_2. As the source is extended, we determine the localization area of the interferences fringes.

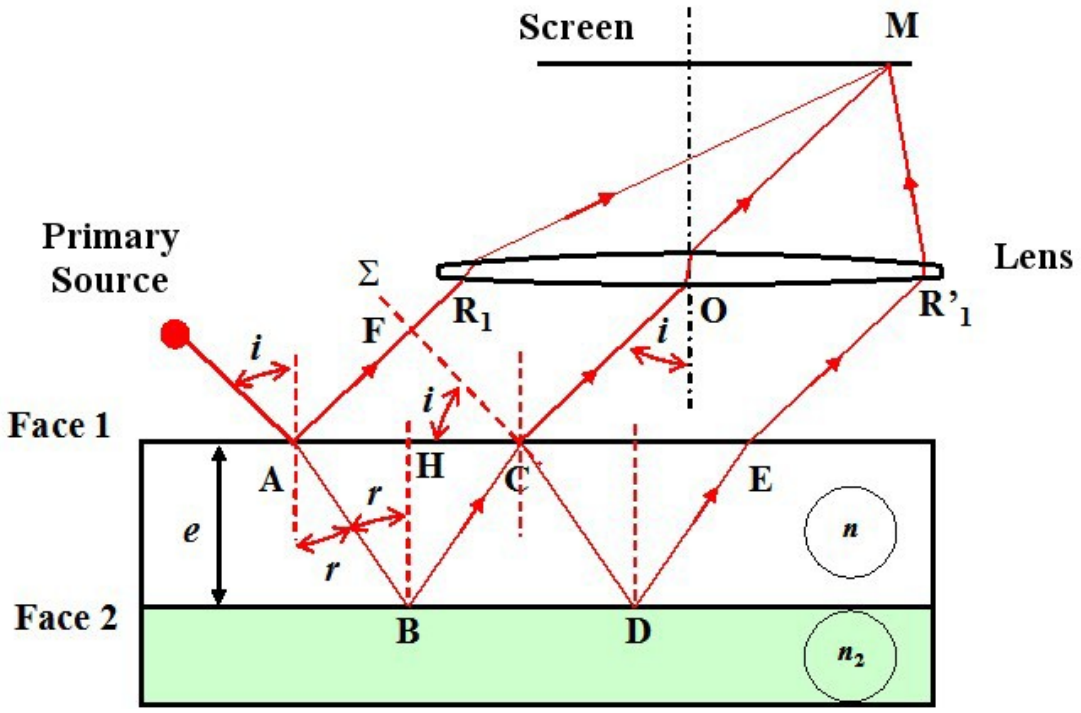

Incident beam SA stemming from primary source S partially reflects in A following the direction AR_1 while a part of refracted beam AB is reflected following BC then refracted in the direction CO. Contributions of beam ER'_1 and following are negligeable because their energy is weak. Indeed, if there is 4% of energy light for the first reflected beam AR_1, there is only 0.0059% for the third beam ER'_1. Both beams AR_1 et CO stemming from the same incident beam SA, emerges parallely between them, they "**interfere at infinity**" . If a screen is located in the image focus plane of a convergent lens, the lens emergent beams cross in M, thus the interference figure is projected on the screen.

As in the case of Young slits, we can express the optical path difference δ in function of the characteristics of the interferometer, which is to say of the plate, as well as the geometrical shape of interferences fringes.

Incident beam SA gives two reflected beams AR_1 and CO. Beyond points C and F both reflected beams follow the same optical path. On the other hand, between A and FC beam AR_1 follows the distance AF in the air and beam CO follows path ABC in the medium with refractive index n. The difference of optical paths between both beams AR_1 and CO equals:

$$[ABC]-[AF]=n(AB+BC)-AF$$

Let us considerer triangle AFC :

$$\sin(i)=\frac{AF}{AC}$$

Hence:

$$AF=AC\sin(i)$$

Let Descartes law be applied for the refraction A :

$$\mathrm{AF}=n\,\mathrm{AC}\sin(r)$$

For triangle ABH we have the following two trigonometric relationships:

$$\tan(r)=\frac{\mathrm{AH}}{e}=\frac{\mathrm{AC}}{2e}$$

Let:

$$\mathrm{AC}=2e\tan(r)$$

And:

$$\cos(r)=\frac{e}{\mathrm{AB}}$$

Let:

$$\mathrm{AB}=\frac{e}{\cos(r)}=\mathrm{BC}$$

Replacing AB, BC and AF by their expressions according to n, e and r in the first equation:

$$[\mathrm{ABC}]-[\mathrm{AF}]=\frac{2ne}{\cos(r)}-2ne\tan(r)\sin(r)=2ne\frac{1-\sin^2(r)}{\cos(r)}=2ne\cos(r)$$

Two different cases have to be considered:

- If the indexes are such as:

$$1<n<n_2$$

Both reflections in A and B are of the same kind, which is to say that each time reflection occurs from a less refringent medium on a more refringent medium. So the course difference δ is equal to the difference of optical path:

$$\delta=2ne\cos(r)$$

- If the indexes are such as:

$$1<n \quad \text{et} \quad n>n_2$$

Reflections are not the same, so we will recognize that, in this case, to add $\lambda/2$ to the course difference δ [1 [[1]]] we have to add to the difference of optical path:

$$\delta=2ne\cos(r)+\frac{\lambda}{2}$$

The points set for which the optical pathdifference is the same are in the same state of interference. The geometrical aspect of the interferences fringes is given looking at the conditions for which $\delta = Cste$.

In the case of bright fringes, interferences are constructive and the course difference δ equals an integer number times the wavelength.

$$\delta = 2\,n\,e\cos(r) = k\,\lambda$$

For a given device, the wavelength, the plate index and thickness are constant and the points in the same state of interference verify:

$$\cos(r) = \text{Cste}$$

As the refraction r and incidence i angles are linked by Descartes law, that leads to $i = Cste$. The observation of interferences figure on a screen E located in the focus image plane of the lens alternately shows bright and dark concentric rings (Figure 6).

Attention

All emergent beams that interfere at the level of a same ring correspond to incident beams that have the same angle of incidence. These interferences fringes are called "same inclination rings".

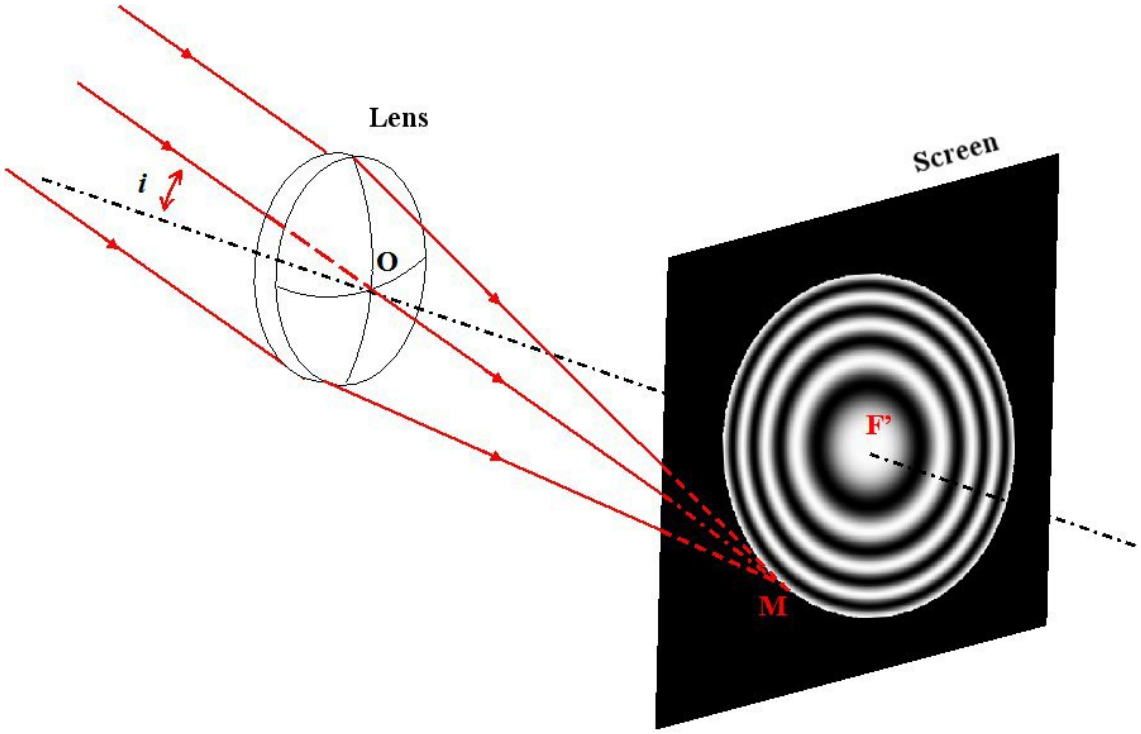

Now we will study angular rays r of the same inclination rings for a plate thickness e. We position ourselves in the case of a bright rings center. In the center, the optical path difference written δ_0 corresponds to a zero angle of reflection r, it is equal to:

$$\delta_0 = 2\,n\,e = k\,\lambda$$

in the case where: $1 < n$ et $n > n_2$

For the peripheral black rings , r raises, the optical path difference δ is smaller than δ_0 and:

$$\delta = 2\,n\,e\cos(r) = k'\,\lambda$$

The interval of optical path difference between a peripheral black ring of order k' and the central ring equals:

$$\delta_0 - \delta = 2\,n\,e(1-\cos(r)) = (k-k')\,\lambda$$

And with a limited expression of cosine for same angles r :

$$\delta_0 - \delta \approx n\,e\,r^2 = (k-k')\,\lambda = K\,\lambda$$

hence:

$$r_K = \sqrt{\frac{K\,\lambda}{ne}}$$

Descartes relation applied to small angles makes the deduction of angle of incidence i_K possible:

$$i_K = n\,r_K = \sqrt{\frac{n\,K\,\lambda}{e}}$$

Remarque

The angular rays of the rings corresponding to the same state of interferences as the center vary as the square root of the successive whole numbers. If the observation is made in the lens focus plane of the image focal distance f', these rings linear radius R are $R_K = f' \tan(i_K)$ (figure 7).

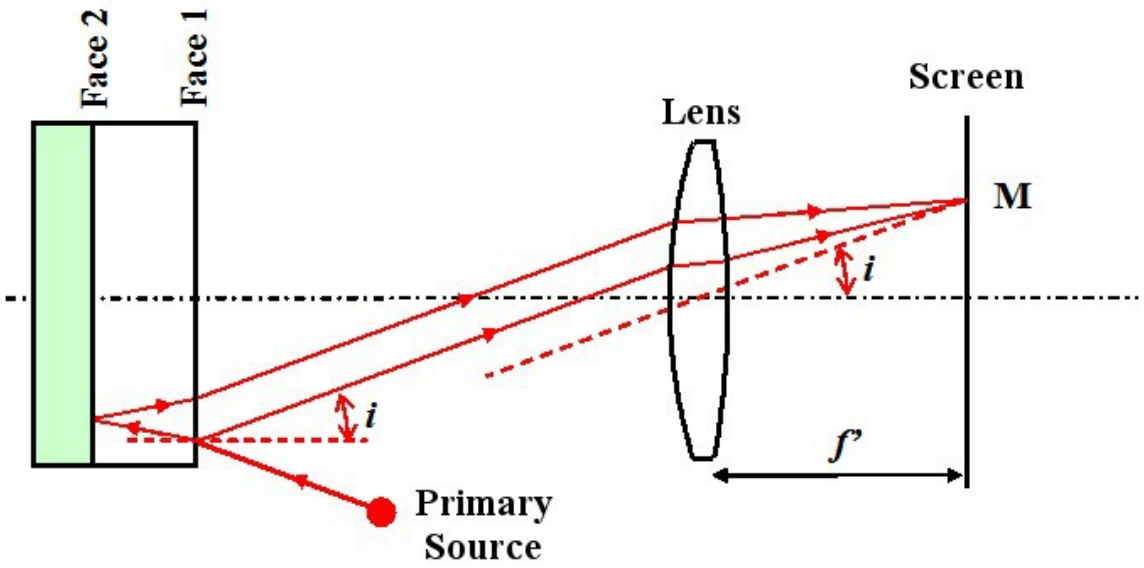

In the air and for small angles, the interfringe is expressed as:

$$\Delta R = R_{K+1} - R_K \approx \sqrt{\frac{n\lambda}{e}} f'$$

2.2. Glass corner

The prismatic plate of apex angle A of index n (figure 8) is illuminated with almost normal incidence by a monochromatic and extended source.

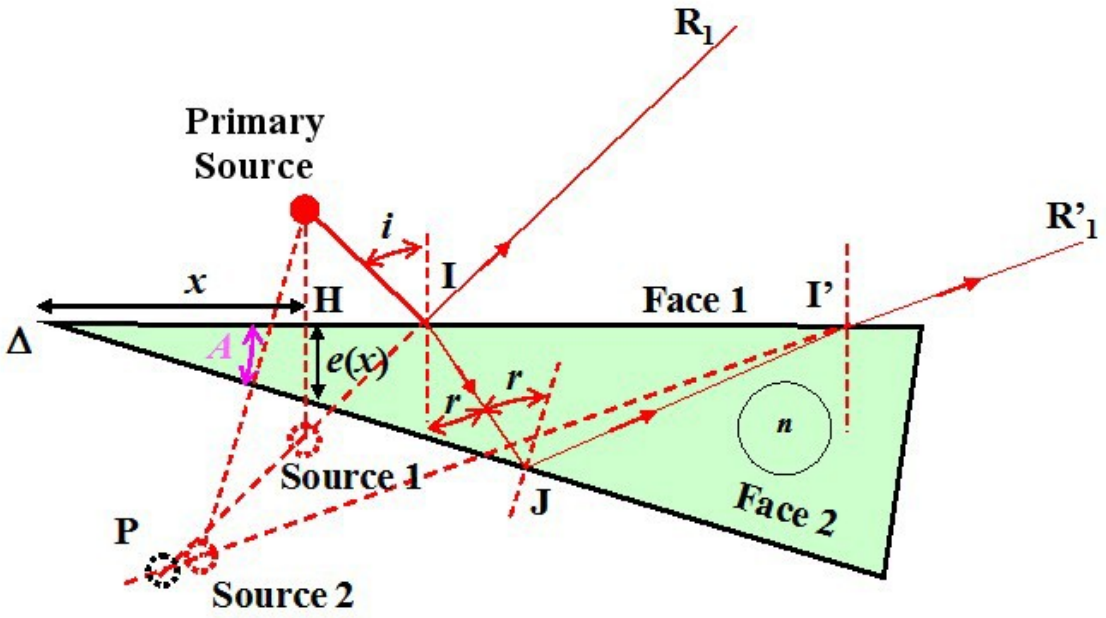

A part of the incident beam SI is reflected on the first diopter surface and a second part is refracted in I then reflected on the second diopter surface in J before it is refracted in I'. Both beams IR_1 and $I'R'_1$ stemming from the same incident beam J converge in P where interfringes are formed. Interferences are located close to the plate, around point P. On figure 8, the incidence angle has been considerably incremented, as well as angle A for more clarity; in reality angle A order of magnitude equals $0.2'$ of arc. In almost regular incidence, points I and I' are very close and the plate thickness can locally be considered as constant and equal to $e(x)$. Thus, the difference of optical path between beams IR_1 and $I'R'_1$ is sensibly equal to the one given by plate with parallel sides placed in the air, lit under normal incidence:

$$\delta = 2ne(x)\cos(r) + \frac{\lambda}{2} \approx 2ne(x) + \frac{\lambda}{2}$$

As the corner index is n, the reflection in I occurs on a more refringent medium than the incident medium when the second reflection in J occurs on a less refringent medium than the incident medium of index n ; both reflections are not of the same kind, which justifies the additional term $\lambda/2$. For any point of a bright interference fringe, the optical path difference verifies:

$$\delta = 2ne(x) + \frac{\lambda}{2} = k\lambda$$

For a given plate, the wavelength and the index are constant; the points corresponding to the same state of interferences, consequently at the same order of interferences k verify:

$$e(x)=\text{Cste}$$

Thus, interferences fringes are lines parallel to the intersection line Δ of both diopters. These fringes are called "**same thickness fringes**". The interfringe Δx is obtained for a variation of order k of one unity hence:

$$e(x)-e(x+\Delta x)=\frac{\lambda}{2n}$$

Considering that $e(x) = x\tan(A) \approx xA$ because angle A is weak, we obtain:

$$\Delta x=\frac{\lambda}{2nA}$$

The interfringe decreases when angle A increases.

Remarque

Both configurations that have just been studied, parallel sides plates and prismatic blades, are particularly important because we can find their concepts in Michelson interferometer and in all interferometers derived from it.

2.3. Michelson interferometer

In its easiest version, a Michelson interferometer is composed of a light source, of two reflecting plane mirrors, of a half-reflecting beam-splitter and of a screen. Figure 9 describes the experimental setup. Mirror 1 is located at distance d_1 from the beam-splitter and mirror 2 at distance d_2. Following both paths, we have two optical systems that play the role of the mirror. For path n° 1: splitter then mirror M_1. So source 1, the image of primary source S, is given by the symmetric of S in relation to the splitter, then by the symmetric in relation to M_1 .The situation is the same on path n° 2 with mirror M_2, then the beam-splitter.

Remarque

At last, the spherical wave emitted by the source is split into two secondary spherical waves stemming from two secondary waves and are propagated towards the screen.

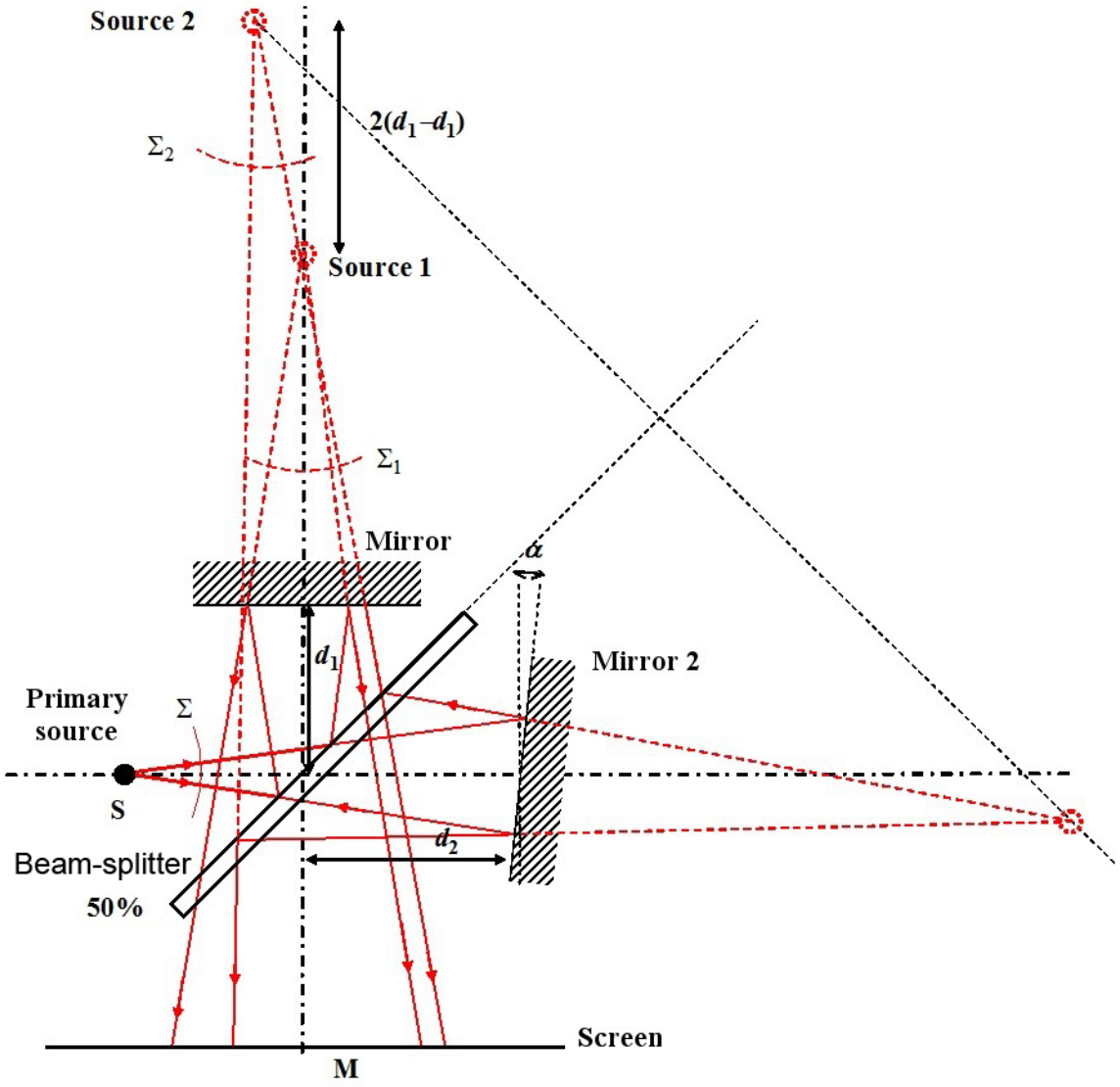

So the setup is equal to a Young holes system as it is described on Figure 10.

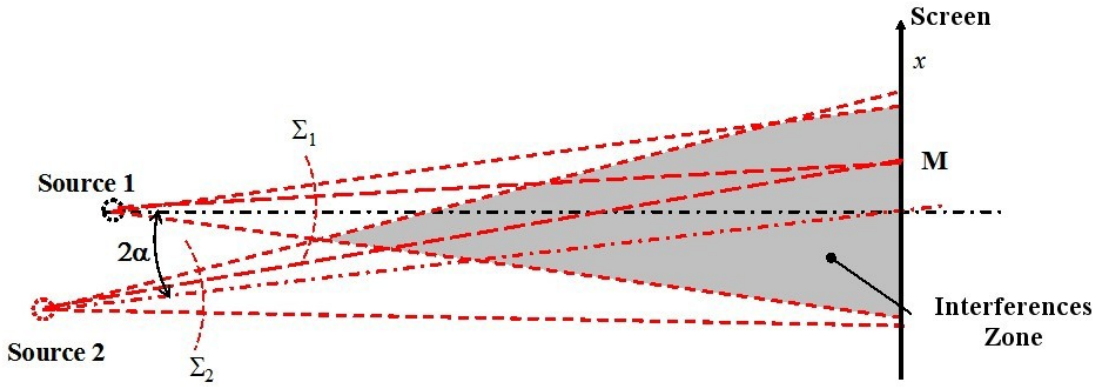

Mirrors are not necessarily located at the same distance from the beam-splitter and the equivalent geometry secondary sources are not necessarily in the same plane or on the same axis. If mirror 2, for example, is switched from an angle α in respect to the optical axis, both secondary sources are also shifted. We are going back to the configuration described in the "**Interferences: Fundamentals**" course. For any point M from the coordinates screen (x, y, z), the interferences phase is:

$$\varphi = \frac{2\pi}{\lambda}\left(\sqrt{(x-x_1)^2+(y-y_1)^2+(z-z_1)^2}-\sqrt{(x-x_2)^2+(y-y_2)^2+(z-z_2)^2}\right)$$

Remarque

If the splitter transmits 50% and reflects 50% of the light, the interference signal is written:

$$I(x,y,z)=\frac{A_0^2}{4r_1^2}+\frac{A_0^2}{4r_2^2}+\frac{1}{2}\frac{A_0}{r_1}\frac{A_0}{r_2}\cos\left(\frac{2\pi}{\lambda}\left(\sqrt{(x-x_1)^2+(y-y_1)^2+(z-z_1)^2}-\sqrt{(x-x_2)^2+(y-y_2)^2+(z-z_2)^2}\right)\right)$$

Where (x_1, y_1, z_1) and (x_2, y_2, z_2) are the coordinates of both secondary sources.

The fringes observed are the ones described in Figure 6 of the "**Interferences: Fundamentals**" course.

Michelson interferometer can also be configured to work with plane waves. In this case, there is just to collimate the initial wave with a lens: The source is placed in the focal point and the mirrors are illuminated in parallel light thus with plane waves. Figure 11 schematizes the setup.

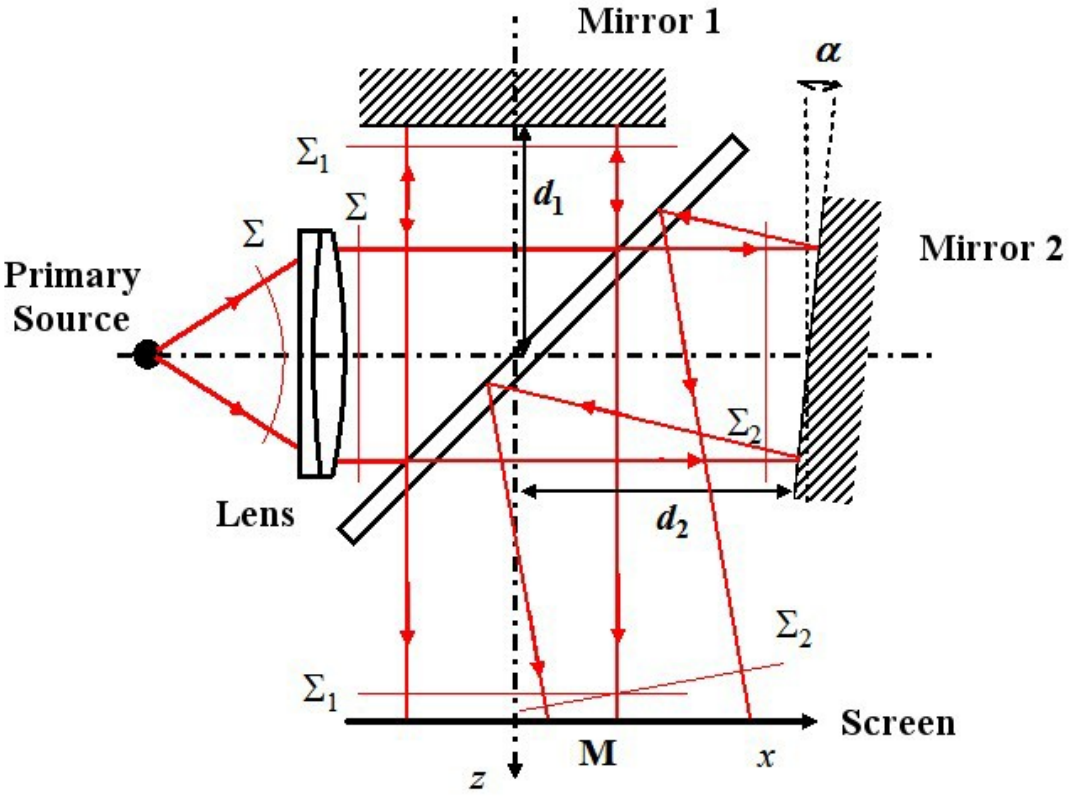

We are in the case treated by paragraph I.B.5 of class "**Interferences: Fundamentals**". Inclinations of mirrors 1 and 2 give the waves vectors of both secondary plane waves. Let us consider that mirror 1 is perpendicular with the optical axis and that mirror 2 is switched from an angle α_x following x and α_y following y. The waves vectors are written:

$$\vec{k}_1 = k_{z1}\vec{e}_z$$

$$\vec{k}_2 = \frac{2\pi}{\lambda}\sin(2\alpha_x)\,\vec{e}_x + \frac{2\pi}{\lambda}\sin(2\alpha_y)\,\vec{e}_y + k_{z2}\vec{e}_z$$

In the plan (x, y), the wave front slopes are $\sin(2\alpha_x)$ and $\sin(2\alpha_y)$. In all points M of the screen, the interferences phase is given by:

$$\varphi = \frac{2\pi}{\lambda}\sin(2\alpha_x)x + \frac{2\pi}{\lambda}\sin(2\alpha_y)y + \frac{2\pi}{\lambda}(d_2 - d_1)$$

And the interferences signal is written:

$$I(x, y, z) = \frac{A_0^2}{2}\left(1 + \cos\left(\frac{2\pi}{\lambda}\sin(2\alpha_x)x + \frac{2\pi}{\lambda}\sin(2\alpha_x)y + \frac{2\pi}{\lambda}(d_2 - d_1)\right)\right)$$

The interfringe following x is given by:

$$\Delta x = \frac{\lambda}{2\sin(2\alpha_x)}$$

And the interfringe following y is given by:

$$\Delta y = \frac{\lambda}{2\sin(2\alpha_y)}$$

Figure 12 shows the spatial field of interferences in the superposition area of both waves in function of mirror 2 inclination in both directions x and y (namely α_x and α_y).

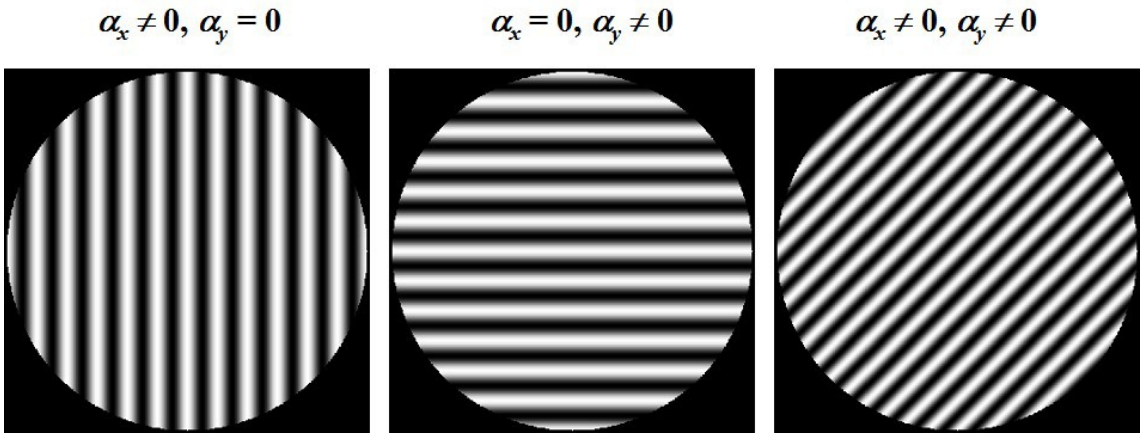

2.4. Mach-Zehnder interferometer

Mach-Zehnder interferometer is composed of a light source, of a collimator, of two reflecting plan mirrors, of two beam-splitters and a screen. The interferometer geometry imposes its symmetry. Figure 13 describes the experimental setup.

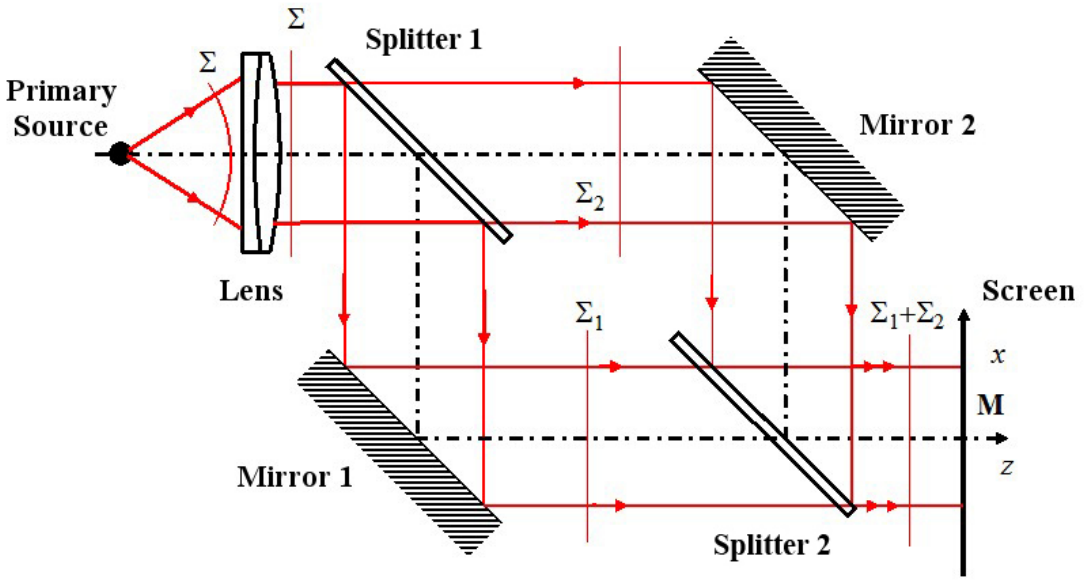

We can note an analogy with the Michelson case with plane waves. Patterns observed are equal to those of Figure 12 when we turn one mirror or both.

2.5. Fizeau interferometer

A Fizeau interferometer is composed of a source of light, of a collimator, of a reflecting plane mirror, of a beam-splitter, of a gauge and of a screen (figure 14). The "gauge" is a glass corner whose sides are perfectly flat and whose face exposed to the plane mirror represents the interferometer second plane mirror. The light reflected on the angle side is suppressed and does not go back to the screen.

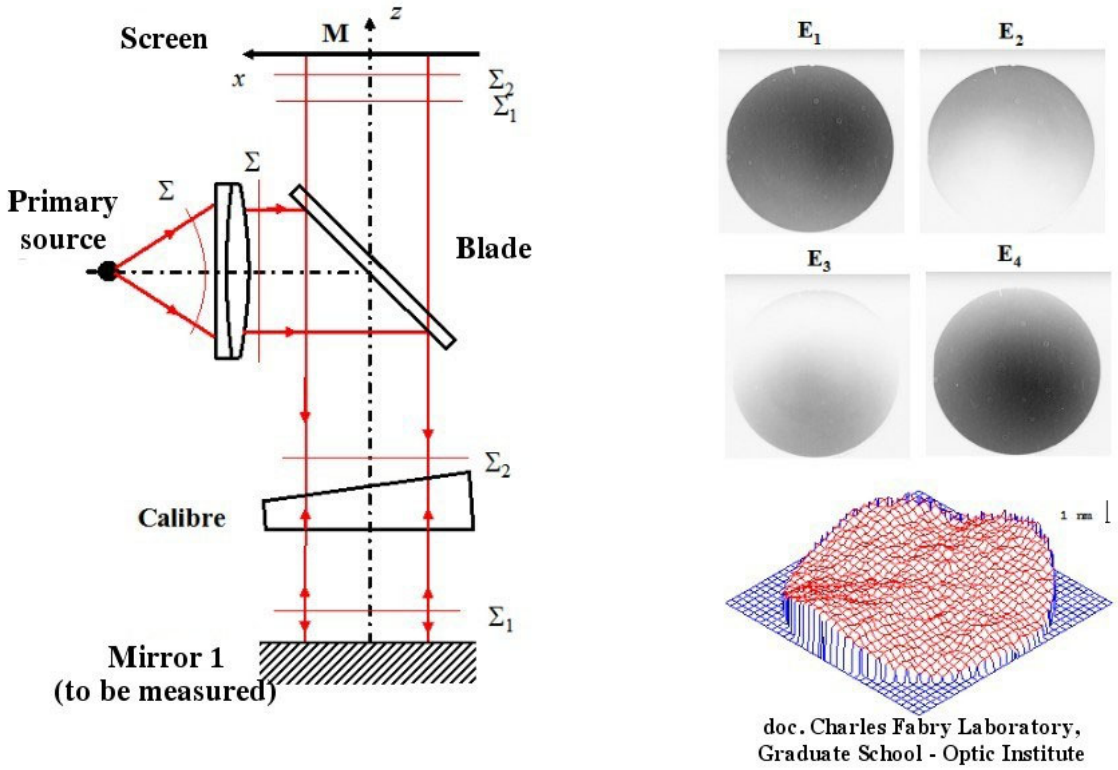

Figure 14 (right part) shows an application of Fizeau's interferometer to smooth surfaces control with a nanometric accuracy, using the phase shifting method (E_1, E_2, E_3, E_4 : interferogram with phase difference of $\pi/2$).

Because of its geometry, when we turn mirror 1 of an angle α, interference fringes observed with the Fizeau equal those of figure 12.

As the air thickness in the cavity of the Fizeau can be reduced to a thin air plate by moving both surfaces close together, this interferometer presents a great advantage for the high precision metrology in comparison with Michelson and Mach-Zahnder ones. Indeed, the air thicknesses in both arms of both interferometers are very large and above all separated so that those interferometers are very sensitive to any disturbance and to the stratification of the air refractive index.

2.6. Sagnac interferometer

Sagnac interferometer is made of a ring architecture as it can be observed in figure 15.

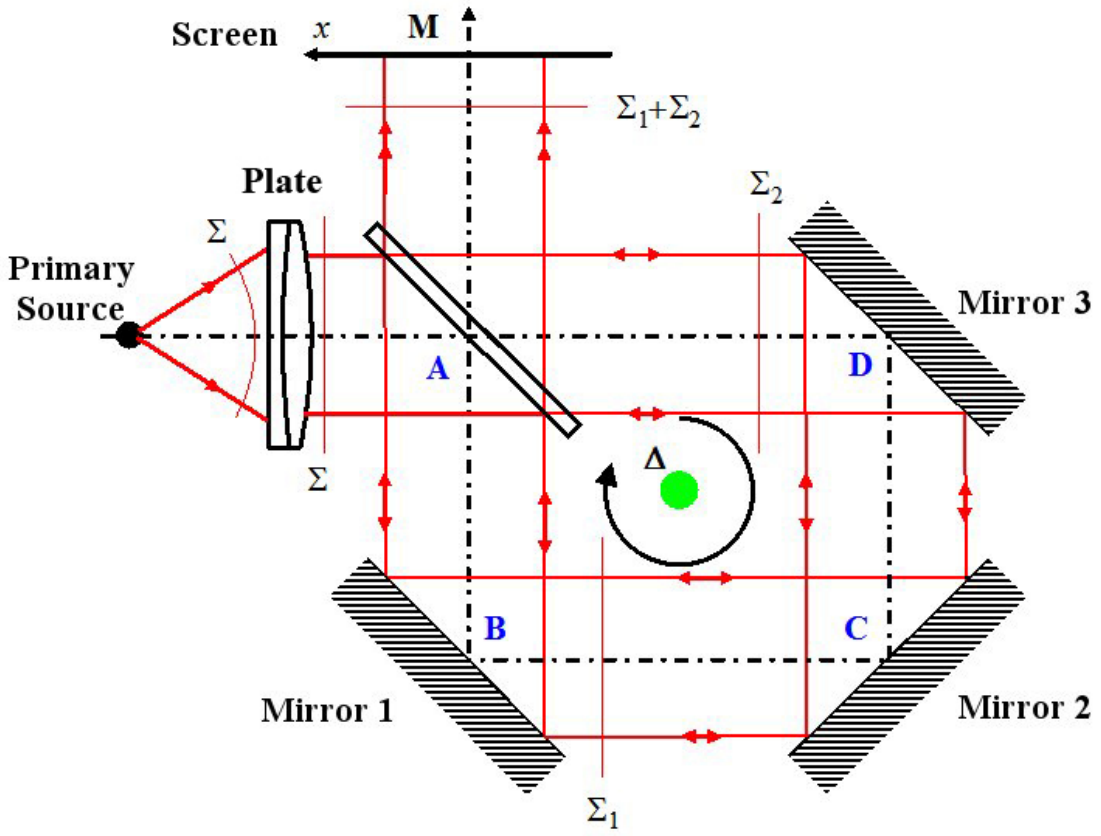

The interferometer input and output spot is A. Both plane waves propagate according to (A, B, C, D, A) and (A, D, C, B, A) paths and so are **contra-propagative**. They follow identical paths. For wave n°1 the optical phase between the input and the output is

$$\varphi_1 = \frac{2\pi}{\lambda}[\mathrm{ABCDA}]$$

And the one for wave 2 is:

$$\varphi_2 = \varphi_1$$

Thus, the phase difference between both waves is zero:

$$\varphi_2 - \varphi_1 = 0$$

Attention

Because of the interferometer symmetry, any switch of one of the three mirrors has no influence on the fringes pattern as the optical paths are all the same on the phase front. The difference of optical path between both waves is constant and zero.

As a consequence, the interference signal is written

$$I(x, y, z) = \frac{A_0^2}{2}(1+\cos(0)) = A_0^2$$

The fringe pattern is uniform: It has a **pale tone**.

This interferometer is of interest in the case where the cavity is in rotation around an axis Δ perpendicular to the figure plane. We can observe that in this case both light beams are phase shifted at the interferometer output: the phase difference depends on the angular speed of rotation ω, of the speed of light c and of the cavity surface S according to the relationship

$$\varphi = \frac{2\pi}{\lambda}\frac{4\omega S}{c}$$

As there is not a strong effect, we are used to gyring a large number of turns N of surface S in order to amplify the output signal.

Exemple

For a loop equals to $R = 10\ \text{cm}$, $\omega = 0,1\ \text{rad/s}$ and $N = 3000$, namely a fiber optic length of $1800\ \text{m}$, we obtain a course difference of $\lambda/4$.

This effect is referred to as "Sagnac effect" and is used in fiber optic laser gyrometer [2 [[2]]]. Fiber gyrometer sensitivity makes the detection of rotation errors of $10^{-3}/h$ possible.

3. Case of multiple-wave interferometer

We are in the case of temporally and spatially coherent sources. A multiple-wave interferometer makes the superposition of a multitude or even an endless number of waves, all phase shifted. If the phase relation between all the waves is perfectly deterministic the fringes pattern can have remarkable properties. In the case where the phase relation between all the waves is random, the resulting pattern is a "**speckle**". The speckle will not be discussed in this course.

The case of the deterministic phase relation is studied later in the course when the complex amplitude relationship between the waves is a geometric progression.

3.1. Multiple-wave interferometer

A simple device can be made of a thickness e and of refractive index n glass plate illuminated by a monochromatic source emitting plane waves. Figure 16 illustrates the interferometer geometry. The incident plane wave is reflected and transmitted a multitude of times.

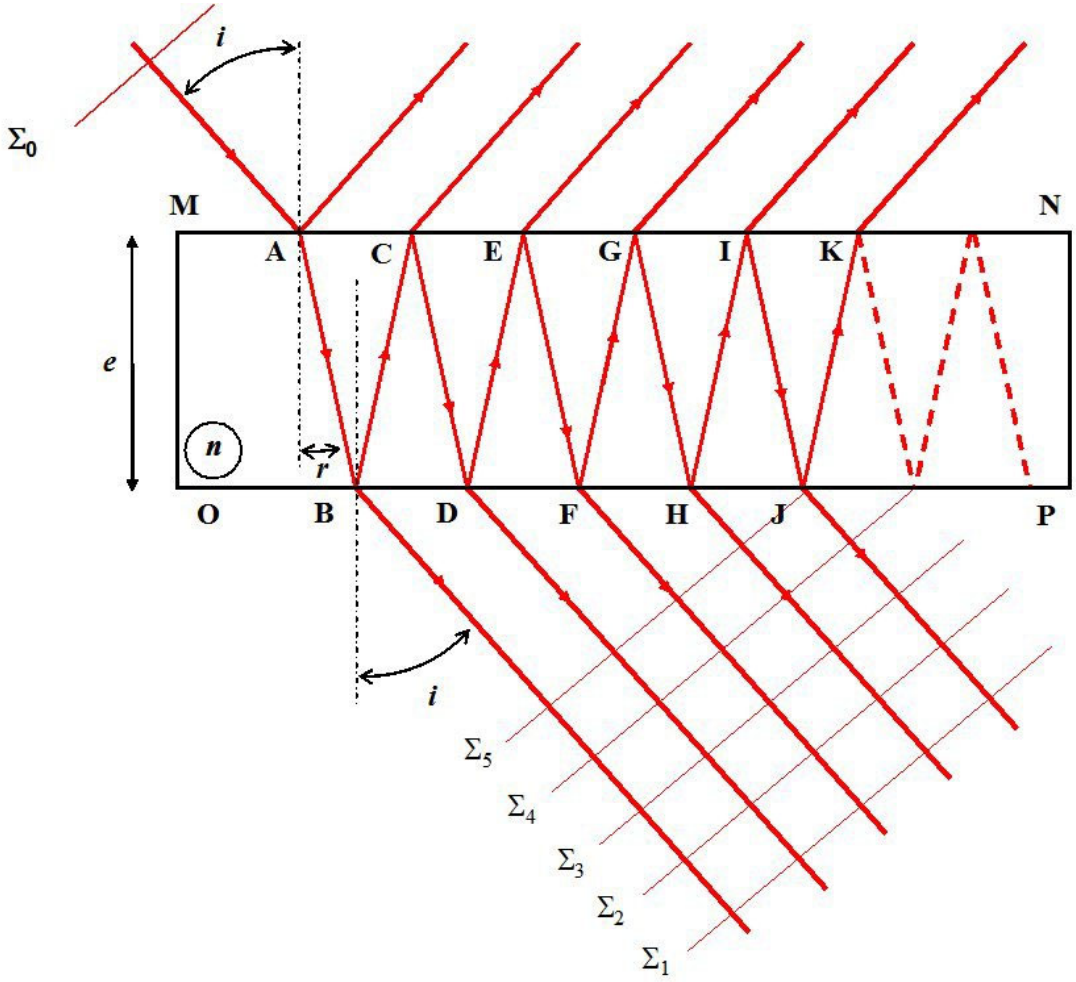

We can write r and t transmission factors in waves amplitude at the air-glass interfaces. The reflection coefficient $R = r^2$ is considered very high, to the order of 99%, so that we do not consider, here, the simple case of the plate with only the first two beams (see Figure 5). Moreover, transmission and reflection coefficients are equal for both diopters. Angles i and r are linked by Descartes relation $\sin(i) = n\sin(r)$. The difference of optical path between two consecutive transmitted waves equals [1 [[1]].3 [[3]]]:

$$\delta = 2\,n\,e\cos(r)$$

In reflection, we have:

$$\delta = 2\,n\,e\cos(r) + \frac{\lambda}{2}$$

Thus, in transmission, the **phase difference between two consecutive waves** is:

$$\varphi = \frac{2\pi\delta}{\lambda} = \frac{4\pi}{\lambda}\,n\,e\cos(r)$$

In output of the plate, in reflection or transmission, the complex amplitude is the sum of all the waves emitted or reflected by the plate. We just have to write down the complex amplitudes that interfere taking the first wave Σ_1 as the phase origin. Let us considerer that the incident wave is flat, polarized according to $\vec{e_x}$, with wave vector $\vec{k_0}$, we have:

$$\vec{E}_0(\vec{r},t)=A_0\exp\left[i\left(\vec{k}_0.\vec{r}-\omega t\right)\right]\vec{e}_x$$

After the plate, we obtain:
For Σ_1:

$$\vec{E}_1(\vec{r},t)=t^2\,A_0\exp\left[i\left(\vec{k}_0.\vec{r}-\omega t+\varphi_0\right)\right]\vec{e}_x$$

Because the wave crosses both diopters MN and OP in A and B.
For Σ_2:

$$\vec{E}_2(\vec{r},t)=t^2r^2\,A_0\exp\left[i\left(\vec{k}_0.\vec{r}-\omega t+\varphi_0+\varphi\right)\right]\vec{e}_x$$

Because of air-glass interface crossing twice in A and D and double reflection at the interface B and C and phase difference φ is related to the first wave;
For Σ_3:

$$\vec{E}_3(\vec{r},t)=t^2r^4\,A_0\exp\left[i\left(\vec{k}_0.\vec{r}-\omega t+\varphi_0+2\varphi\right)\right]\vec{e}_x$$

Because of crossing twice in A and F and four reflections in B, C, D, E which correspond to a difference of phase of 2φ compared to the first wave.

Attention

with a recurrence, we can observe that for Σ_n :

$$\vec{E}_n(\vec{r},t)=t^2r^{2n-2}\,A_0\exp\left[i\left(\vec{k}_0.\vec{r}-\omega t+\varphi_0+(n-1)\varphi\right)\right]\vec{e}_x$$

The full complex amplitude at output of the plate results from the sum of all the amplitudes:

$$\vec{E}(\vec{r},t)=\vec{E}_1(\vec{r},t)+\vec{E}_2(\vec{r},t)+\ldots+\vec{E}_n(\vec{r},t)+\ldots$$

We put down $T=t^2$ and $R=r^2$, T and R are transmission and reflection in optical intensity (or power, or energy).
The complex fields summation gives:

$$\vec{E}(\vec{r},t)=T\,A_0\exp\left[i\left(\vec{k}_0.\vec{r}-\omega t+\varphi_0\right)\right]\left[1+Re^{i\varphi}+R^2e^{i2\varphi}+\ldots+R^ne^{in\varphi}+\ldots\right]\vec{e}_x$$

We recognize a geometric sequence of common ratio $q=Re^{i\varphi}$ and of first term 1. Let N be the total number of terms, we have for the sum:

$$1+Re^{i\varphi}+R^2e^{i2\varphi}+\ldots+R^ne^{in\varphi}+\ldots=\frac{1-R^Ne^{iN\varphi}}{1-Re^{i\varphi}}$$

And according to $R = r^2$ is less than 1, $\lim_{N\to\infty} |q|^N = 0$, it remains:

$$1+R\,e^{i\varphi}+R^2\,e^{i\,2\varphi}+\ldots+R^n\,e^{i\,n\varphi}+\ldots=\frac{1}{1-R\,e^{i\varphi}}$$

The interferences signal is proportional to:

$$I(\vec{r},t)=\left|\vec{E}(\vec{r},t)\right|^2$$

Hence :

$$I(\vec{r},t)=\frac{T^2\,A_0^2}{\left|1-R\,e^{i\varphi}\right|^2}$$

That we write:

$$I(\phi)=\frac{T^2\,A_0^2}{1+R^2-2\,R\cos(\varphi)}$$

As $\cos(\varphi) = 1 - 2\sin^2(\varphi/2)$, we get:

$$I(\phi)=\frac{T^2\,A_0^2}{(1-R)^2+4\,R\sin^2\left(\frac{\varphi}{2}\right)}$$

Let us put down: $m = \frac{4R}{(1-R)^2}$, and $I_0 = A_0^2$
With $T = 1 - R$
Here comes:

$$I(\phi)=\frac{I_0}{1+m\sin^2\left(\frac{\varphi}{2}\right)}$$

The minimum and maximum values of the signal are

$$I_{\min}=\frac{I_0}{1+m} \qquad I_{\max}=I_0$$

And the contrast is worth

$$C=\frac{I_{\max}-I_{\min}}{I_{\max}+I_{\min}}=\frac{m}{m+2}$$

Figure 17 illustrates the interferences signal $I(\varphi)/I_0$ in transmission in function of coefficient of reflection R for different values.

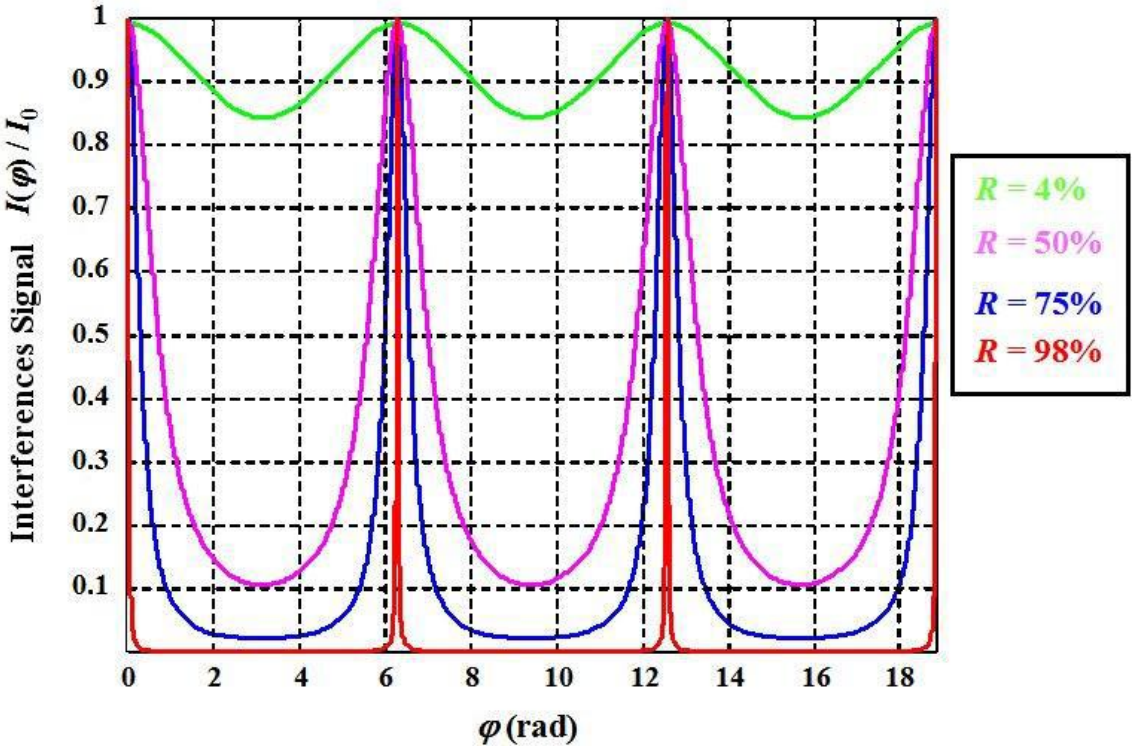

We can observe that the higher the coefficient of reflection is, the further the fringe profiles from the classical sinusoidal profile are. For $R > 98\%$, the profile becomes more refined and constitutes a filtering function whose properties will be used in the "**Case study**". The case $R = 4\%$ corresponds to the case of a 1.5 index glass plate and was developed above in paragraph I.B.1.

Let us imagine that the incident light on a Fabry Perot interferometer is polychromatic. If the light spectrum is composed of a very thin doublet, both peaks are then very close to each other, they can be distinguished if they are very thin as the peaks represented in red color (Figure 17).

Remarque

The **free spectral interval of the interferometer** corresponds to the wavelength variation $\Delta\lambda = \lambda_2 - \lambda_1$ for which there is a superposition of the consecutive peaks of order k for the wavelength λ_2 and of order $k+1$ for λ_1 namely:

$$\frac{4\pi}{\lambda_1} n e \cos(r) = 2(k+1)\pi$$

And :

$$\frac{4\pi}{\lambda_2} n e \cos(r) = 2k\pi$$

Hence we can make the deduction:

$$4\pi n e \cos(r)\left(\frac{1}{\lambda_1} - \frac{1}{\lambda_2}\right) = 2\pi$$

As $\Delta\sigma = \frac{1}{\lambda_1} - \frac{1}{\lambda_2}$, we can deduce the expression of the free spectral range:

$$\Delta\sigma = \frac{1}{2ne\cos(r)}$$

According to the expression $I(\varphi)/I_0$, the half-height width of the interferometer resonance peaks equals to:

$$\delta\sigma = \frac{1-R}{2\pi ne\sqrt{(R)}\cos(r)}$$

From both expressions we define the **interferometer finesse** by:

$$F = \frac{\Delta\sigma}{\delta\sigma} = \frac{\pi\sqrt{(R)}}{1-R}$$

Those parameters are illustrated on figure 18.

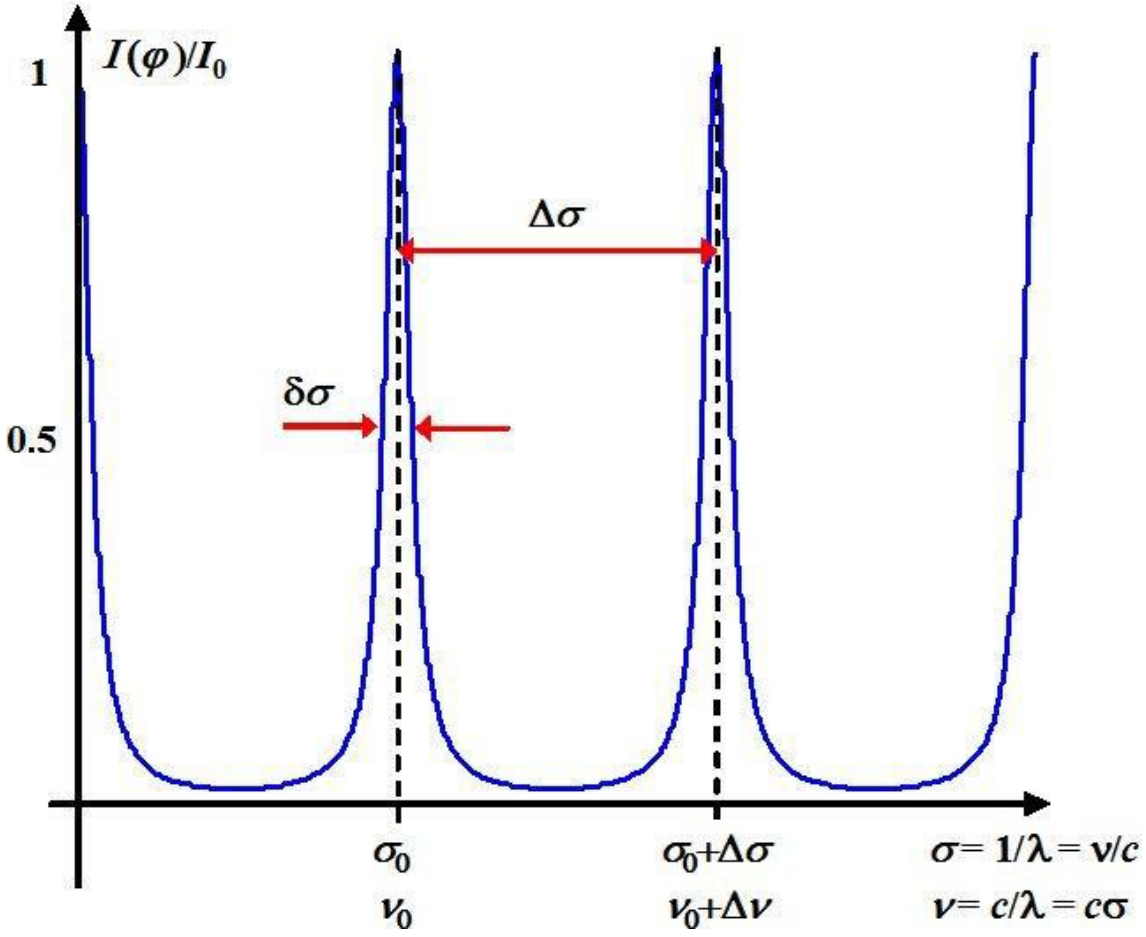

Table 1 gives values of modulation, contrast and thinness parameters as a function of the coefficient of reflection.

Coefficient of reflection (R)	Modulation (m)	Contrast (C)	Thinness (F)
4.00%	0.15	6.88%	0.65
50.00%	8	80.00%	4.44
75.00%	48	96.00%	10.88
98.00%	9800	99.98%	155.5

The reader will note that in the 4% case, we are no longer looking at multiple wave interferences and that we find the same result, seen above, about the parallel sides plate treated in the case of two-wave interferences (Figure 5 and Paragraph I.B.1).

A Fabry Perot interferometer is commonly used for spectral analysis.

It is also often used when it is constituted of a thickness e air plate and of glass corners which faces, constituting the glass plate, are treated for the reflection coefficient to be very high and close to 1. Thus we talk about "**etalon**". That kind of system is used in laser cavities in order to spectrally refine and make the source single mode and longitudinal, that is to say coherent. Figure 19 presents the schematic diagrams as well a gage block picture.

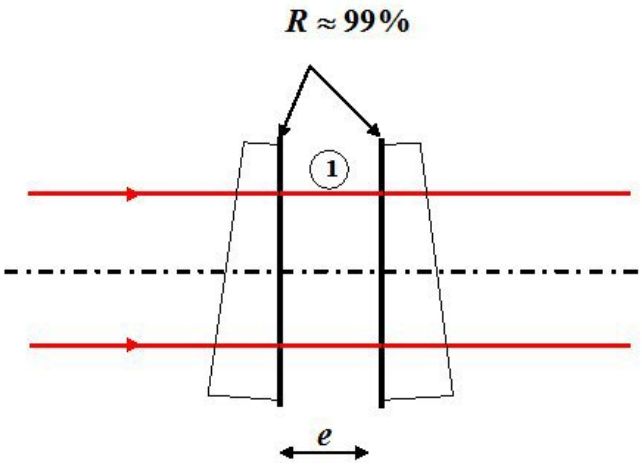

3.2. Differential interferometers

Differential interferometers (also called **lateral shift interferometers** or shearing interferometers) are an often unknown component of interferometry but constitute an important field in various applications such as surfaces and optical system inspections or fluid and turbulences in gas and liquids studies.

The basic principle is to make interferences between the initial wavefront and its copy, laterally shifted of a small quantity [4 [[4]]]. Figure 20 illustrates the principle. We are used to laterally shift the wavefront without changing its shape. The optical components used in the interferometer are often semi-reflecting beam-splitters.

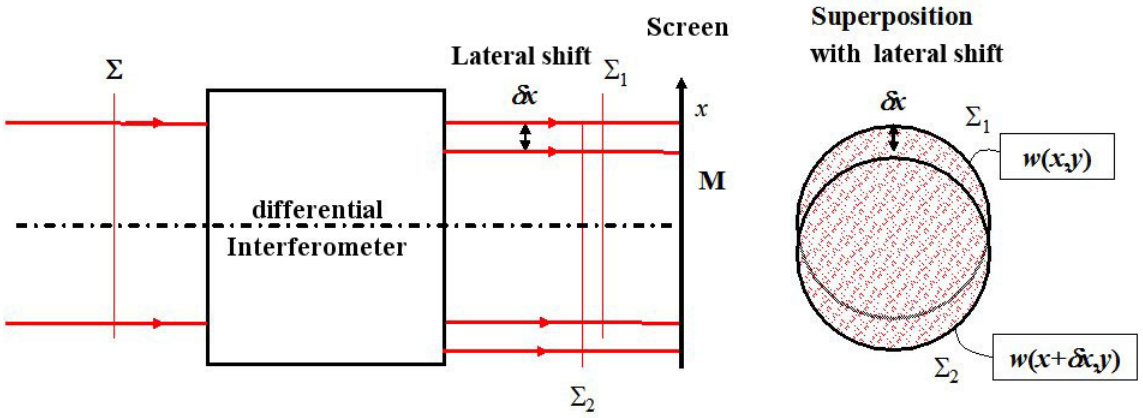

Remarque

Let us write $w(x,y)$ the wavefront in $\mathbf{M}$ in the screen plane. The laterally shifted wave front according to x, for instance, of a quantity δx is simply $w(x+\delta x,y)$. The difference in an optical phase made by both wavefront interferences is given by:

$$\varphi(x,y)=\frac{2\pi}{\lambda}\left[w(x+\delta x,y)-w(x,y)\right]$$

Because of the mathematical definition of the derivative, the difference of phase is also written:

$$\varphi(x,y)\approx\frac{2\pi}{\lambda}\delta x\frac{\partial w(x,y)}{\partial x}$$

Complément

Thus, the information contained by the interferogram is relating to the wavefront derivative in the lateral shift direction; so it is linked to the wavefront slops in the shift direction.

Various experimental architectures exist to make a shearing interferometer [4 [[4]]]. A simple way is to use a Mach-Zehnder type interferometer in which we have two parallel and plane sides glass plates each one inserted into each one of the interferometer arm. If the two blades are perfectly parallel, then both wavefronts are released perfectly superimposed from the interferometer and we can observe a pale tone as the phase difference is null. On the contrary, if we tilt plate n° 1, for example, of an angle α, wavefront n° 1 is now laterally shifted of δx . Thus, both wavefronts interfere in a differential mode. Quantity δx can be adjustable in function of the tilting angle. Indeed, for small angles, the lateral shift is given by:

$$\delta x\approx e(n-1)\alpha$$

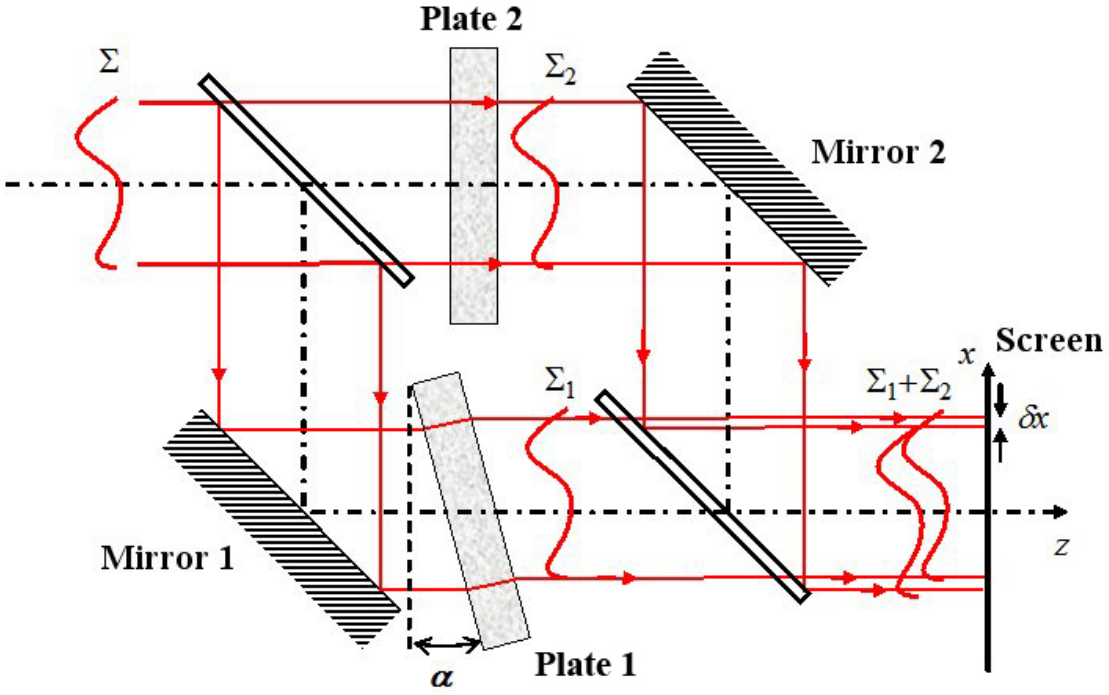

Other experimental solutions exist to make a differential interferometer. For further information, the reader should read reference [4 [[4]]].

* *

*

Interferometry is a measurement technique applied to a large variety of fields of physics: length, temperatures, pressures, forces, angular speeds and spectroscopy measurements. As resolution limits can be very weak, it is a favorite technique in meterology. During "precision" measurements, due to the high sensitivity of the method, we will have to make sure that we take into account every parameter that could have an influence on a measurement such as vibrations and temperature and optical paths stability.

This course has distinguished two different types of interferometers; the wavefront-splitting ones which an essentially historical and educational interest and the amplitude-splitting ones used more often as they are brighter. Most of the latter ones are derivatives from the Michelson interferometer.

III.Case study

This casework deals with the Twyman-Green interferometer used to control optical systems as well as with Fabry Perot spectrometers. The last case is that of Fourier transform spectrometry.

1. Twyman-Green interferometer

The Twyman-Green interferometer is a modified version of the Michelson interferometer. It is used industrially for the interferometric control of non-plane optical surfaces and mirrors or lens objectives. Figure 22 presents the Twyman-Green set-up.

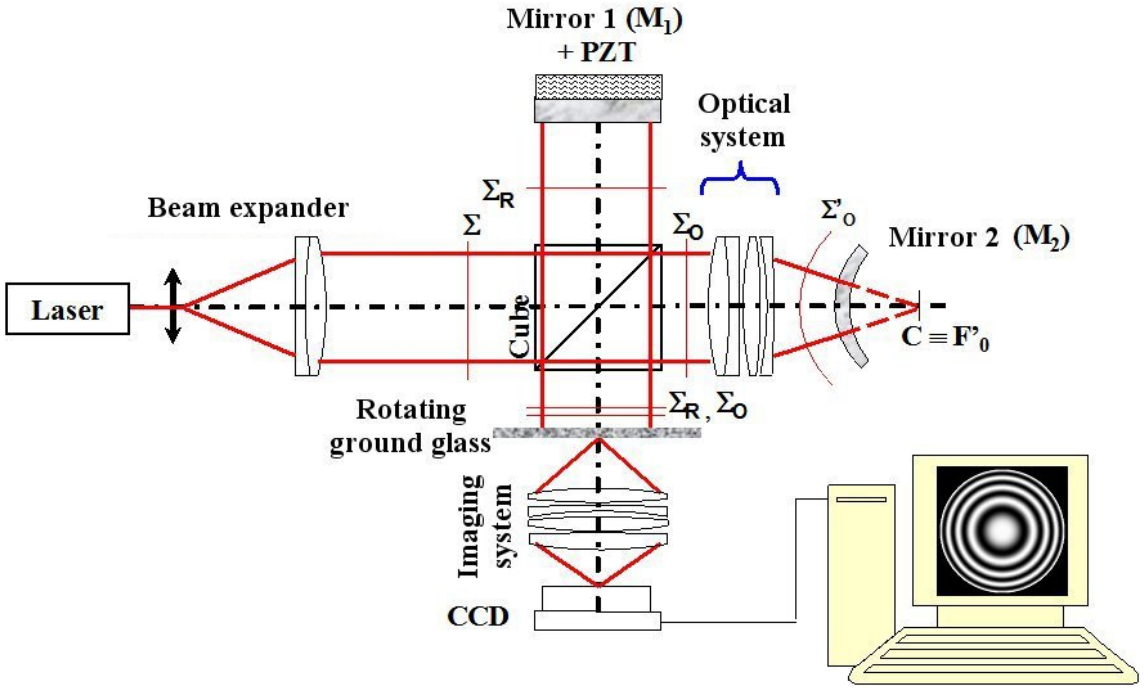

The Michelson plane mirror M_2 is replaced by a combination of the optical system to be studied and a spherical mirror. The spherical mirror is placed for its curvature center C to be superimposed with the paraxial focus of the optical system F'_0. At the output of the interferometer, the fringes are visible on the screen that is now replaced by a rotating ground-glass. The optical imagery system creates the fringes image on the CCD or CMOS matrix detector. If the ground-glass were static, it would generate a **speckle** (random phenomenon) that would destroy the interference fringes. Thus, the ground-glass is usually assembled on a motor that makes it rotate fast enough for the speckle to be averaged in the integration time of the image sensor. So that the speckle grains are no longer visible anymore on the fringe pattern.

Reference plane mirror (M_1) is mounted on a piezoelectric transducer which makes it possible to translate M_1 and to apply the phase shift method in order to calculate the interference optical phase. This interferometer aspect will not be detailed here but the reader is encouraged to look at the "**Interferometry and fringe demodulation**" course.

Plane wave surface Σ emitted from the laser is split into two plane waves Σ_R and Σ_O. Back and forth on mirror M_1, reference wave surface Σ_R remains flat, but it can possibly be sloped by a tilt of mirror M_1. Object wave surface Σ_O is transformed into a spherical wave by the optical

system, if it is perfect, then by reflection on the spherical mirror and back in the optical system, it is flat again. Interferences between the ideal plane wave from mirror M_1 and the wave front made from the optical system occur at the interferometer output. The interference fringe analysis makes it possible to quantify the defect introduced by the optical system.

1.1. Optical aberration

If the optical system is perfect then the wave front issued from the "optical system + mirror 2" is flat. In the opposite case, it has "**aberration**" due to the optical system [4 [[4]].5 [[5]]]. If the optical system is aberrant then the wave front at the system output is not spherical but has a deviation that is the difference between the real wave front and the ideal spherical wave front (see figure 23).

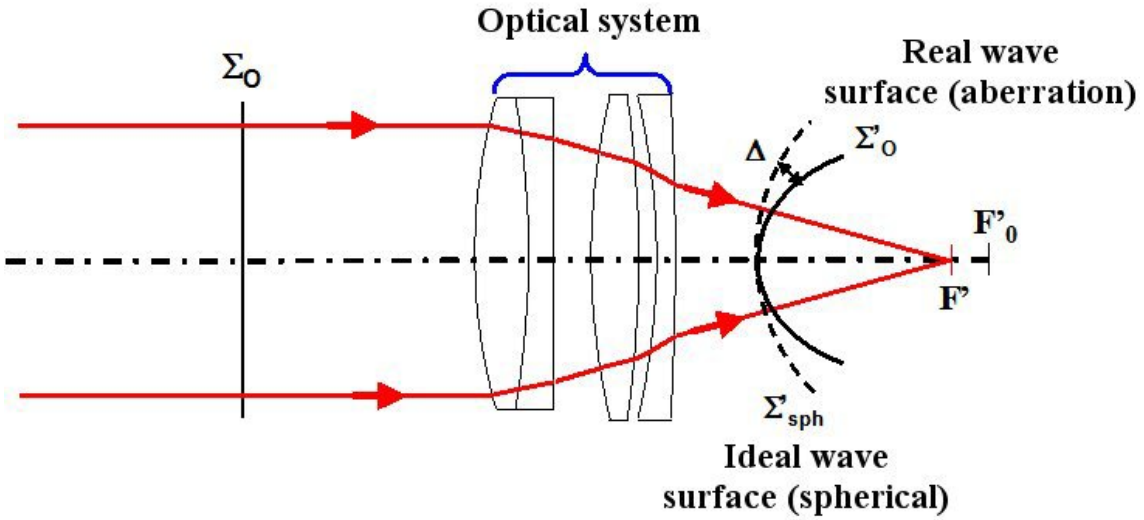

A Twyman-Green interferometer easily highlights the following primary aberrations [4 [[4]].5 [[5]]]:

Third-order spherical aberration

Third-order coma aberration

Third-order astigmatism aberration

The analytic expression of the aberrations is given in the following examples.

Rappel

The aberration always refers to the difference between the real wave front and the reference wavefont that can be either flat or spherical.

1.2. Contribution of both mirrors

The reference arm is composed of plane mirror M_1 mounted on the piezoelectric transducer. A priori, the reflected wave front that interferes with the measuring wavefront is flat but it may be tilted in respect to the ideal plane. That inclination can be made by a tilting of mirror M_1 .The reader can observe that the same thing occurs with a tilting of mirror M_2. If mirror M_1 is slightly translated by the PZT then a uniform phase shift of all the reference wavefront points will occur. Δ_R will be the contribution from the reference arm (M_1 + PZT, back and forth).

In the measurement arm, mirror M_2 can be tilted or translated. Translation of mirror M_2 on each side of the optical system paraxial focus will create a **defocusing**. Thus a contribution of the mirror to the aberration of the optical system-mirror M_2 will be observed. It is also referred as "**focusing defect**".

1.3. General expression of the interferogram

Let us suppose that the polarizations are parallel, so the interferogram is written:

$$I = I_1 + I_2 + 2\sqrt{I_1 I_2}\cos\left(\frac{4\pi}{\lambda}(\Delta_O - \Delta_R) + \varphi_0\right)$$

Where :

- Δ_O is the aberration from the measurement beam (optical system + M_2),
- Δ_R is the contribution from the reference arm (M_1 + PZT),
- φ_0 is the optical phase that corresponds to the total optical path difference between both interferometer paths, at the images sensor plane.

According to the contributions given by the various elements, the interferometer fringes will have different shapes.

In the following, we suppose that $I_1 = I_2 = I_0$, that is to say that the fringes have a maximal contrast equal to 1.

1.4. Interferogram with a perfect optical system

Let us consider that everything is perfect: optical system, mirror M_1 perpendicular to the optical axis and mirror M_2 perpendicular to the axis and not out of focus. So the contributions are $\Delta_0 = \Delta_R = 0$, the interferogram is:

$$I = 2I_0\left(1 + \cos\left(\varphi_0\right)\right)$$

There is no fringe but "**a flat colour**".

As we said it before, the same thing will happen with a tilting of mirror M_1 or M_2 : a wavefront tilt at the output. Let us suppose that the tilting is caused by mirror M_1. In terms of wavefront, tilt results in the equation a plane so that:

$$\Delta_R(x, y) = \sin(\alpha_x)x + \sin(\alpha_y)y$$

where (α_x, α_y) are the mirror tilting angles respectively in directions (x, y). So the interferogram has straight fringes as illustrated on Figure 12.

Let us consider now that mirror M_2 is also slightly defocused by a translation ε along the optical axis. The contribution caused by that defocusing is written [4 [[4]].5 [[5]]]:

$$\Delta_R(x, y) = \epsilon\frac{x^2 + y^2}{2p'^2}$$

This is illustrated on Figure 24.

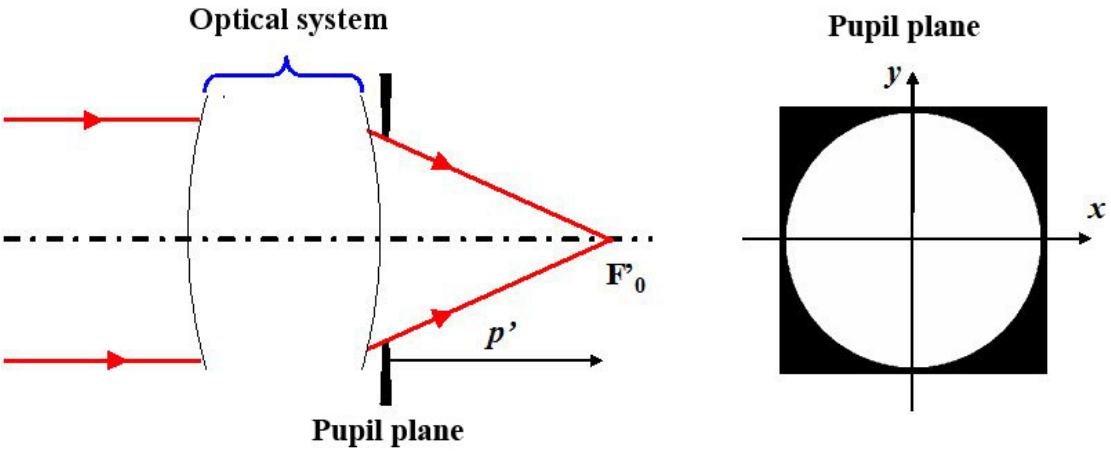

Figure 25 illustrates the wavefront shape and the interferogram obtained with the mirror M_2 defocusing.

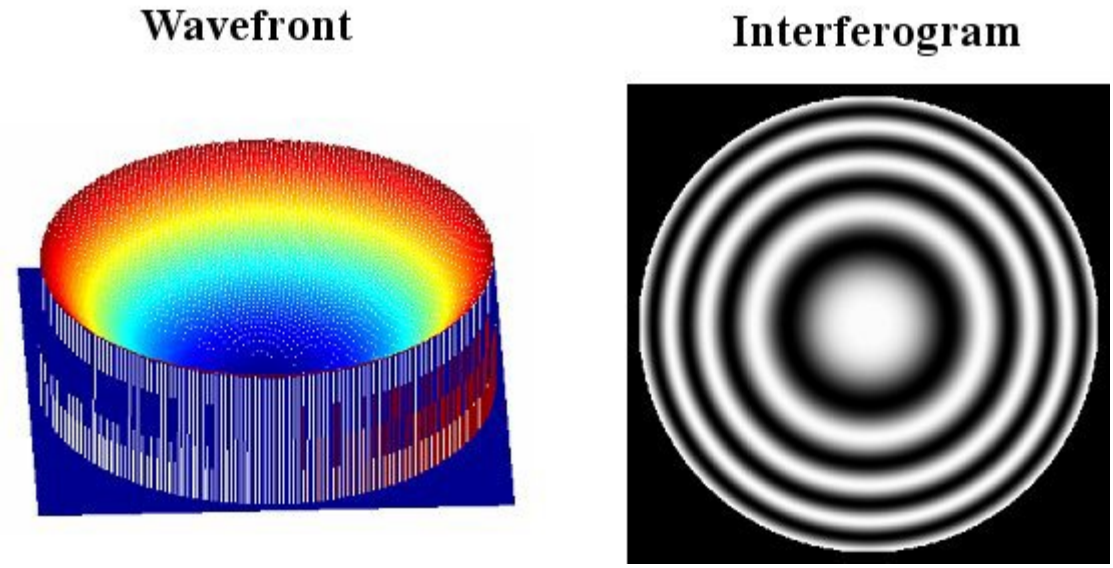

1.5. Interferogram with third-order spherical aberration

The spherical aberration is an **aperture aberration**, that is to say it appears for a image point located on the imager system optical axis whose aperture diameter is wide (numerical aperture wider than 0.35). In the case where the optical system has third-order spherical aberration, the aberration is expressed by the following relation [4 [[4]].5 [[5]]]:

$$\Delta_O(x,y) = -a_1 \frac{\left(x^2+y^2\right)^2}{4\,p'^2}$$

Where a_1 is the coefficient of the third-order spherical aberration.

Figure 26 illustrates the wavefront shape and the interferogram with third-order spherical aberration.

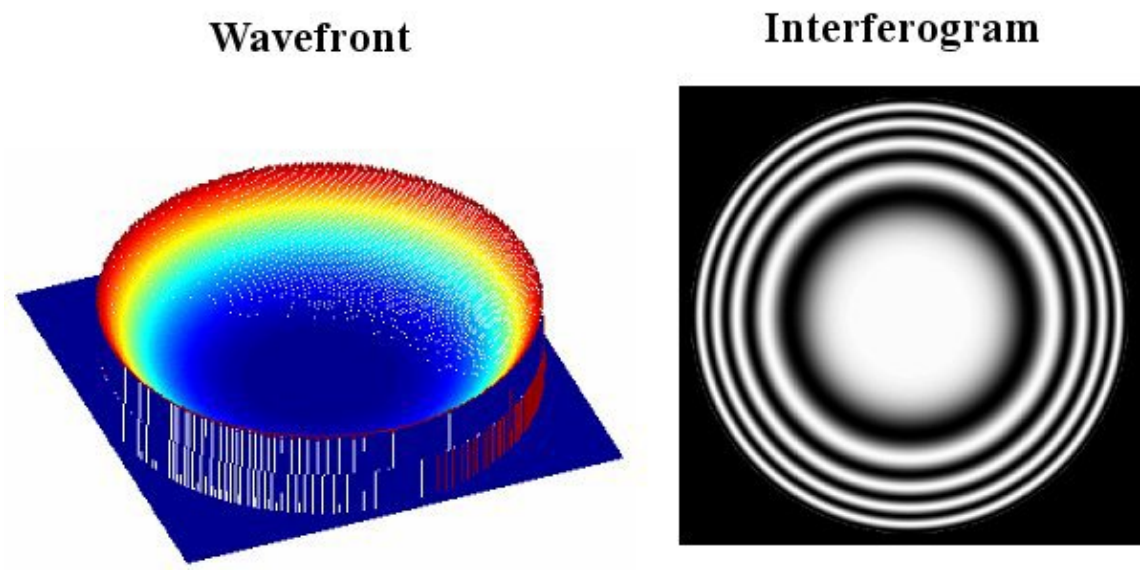

If mirror M_1 is now tilted, the wavefronts difference at the interferometer output becomes:

$$\Delta_O(x,y)-\Delta_R(x,y)=-a_1\frac{\left(x^2+y^2\right)^2}{4\,p'^2}-\sin(\alpha_x)\,x-\sin(\alpha_y)\,y$$

Figure 27 illustrates the wavefront shape and the interferogram with third-order spherical aberration and a tilting of mirror M_1.

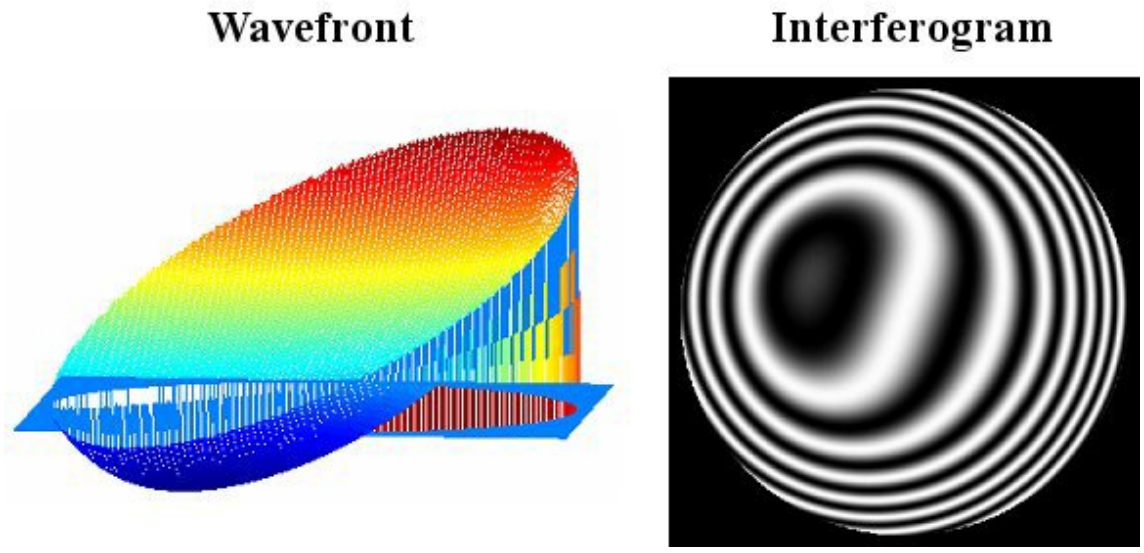

In the case mirror M_2 is slightly defocused, the wavefronts difference at the interferogram output becomes:

$$\Delta_O(x,y)-\Delta_R(x,y)=-a_1\frac{\left(x^2+y^2\right)^2}{4\,p'^2}-\epsilon\frac{x^2+y^2}{2\,p'^2}$$

Figure 28 illustrates the wavefront shape and the interferogram with third-order spherical aberration and a defocusing of mirror M_2.

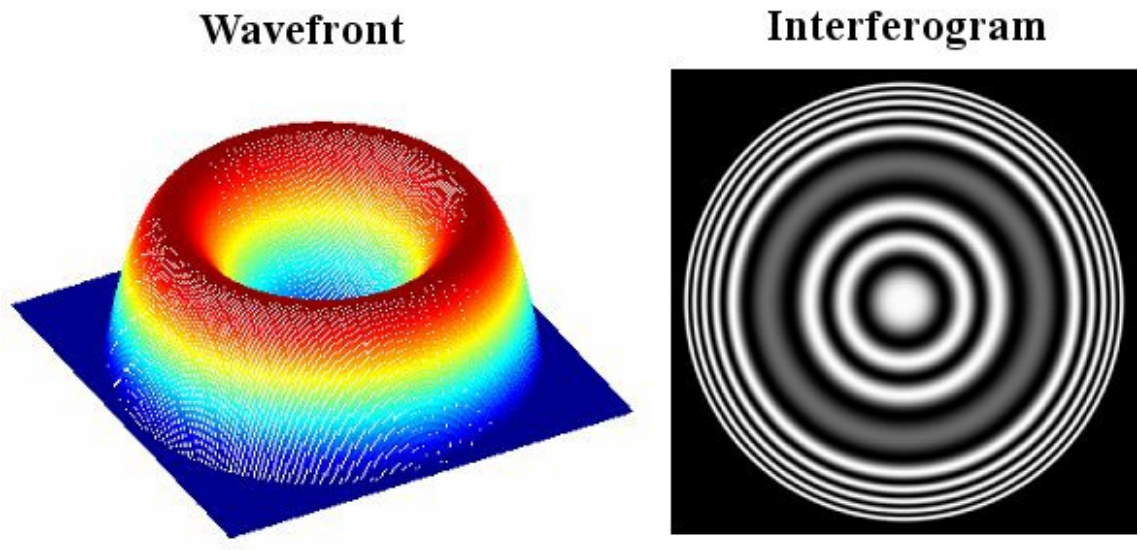

1.6. Interferogram with third-order coma aberration

The coma aberration is a **field and aperture aberration**, that is to say it appears away from the axis. In Figure 22, it is not possible to highlight the coma. The assembly must be adapted in order to simulate an extended image $\overline{A'_0B'_0} = y'$. The optical system must be turned by an angle θ. Thus the incident beams converge towards image point B'_0, that can be confounded with mirror M_2 curvature center. The image size is $y' = -\theta f'$. The coma is expressed by the following relation [4 [[4]].5 [[5]]]:

$$\Delta_O(x,y) = -b_1 y' \frac{y(x^2+y^2)}{p'^3}$$

Where b_1 is the third-order coma aberration coefficient.

Figure 29 shows the experimental configuration for the coma measurement.

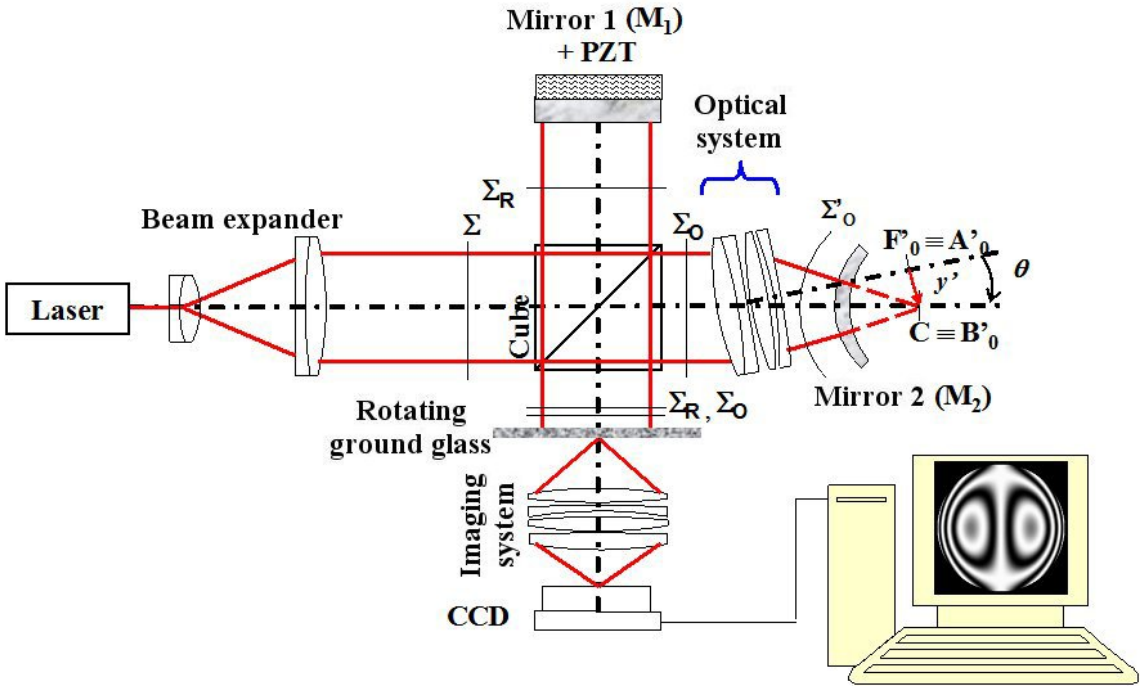

Figure 30 illustrates the wavefront shape and the interferogram with third-order coma aberration. The initial configuration is done in the case where the paraxial image is confounded with the M_2 curvature center: we can also move the curvature center in the coma spot and study the aberration. That move will be done by tilting the mirror M_2.

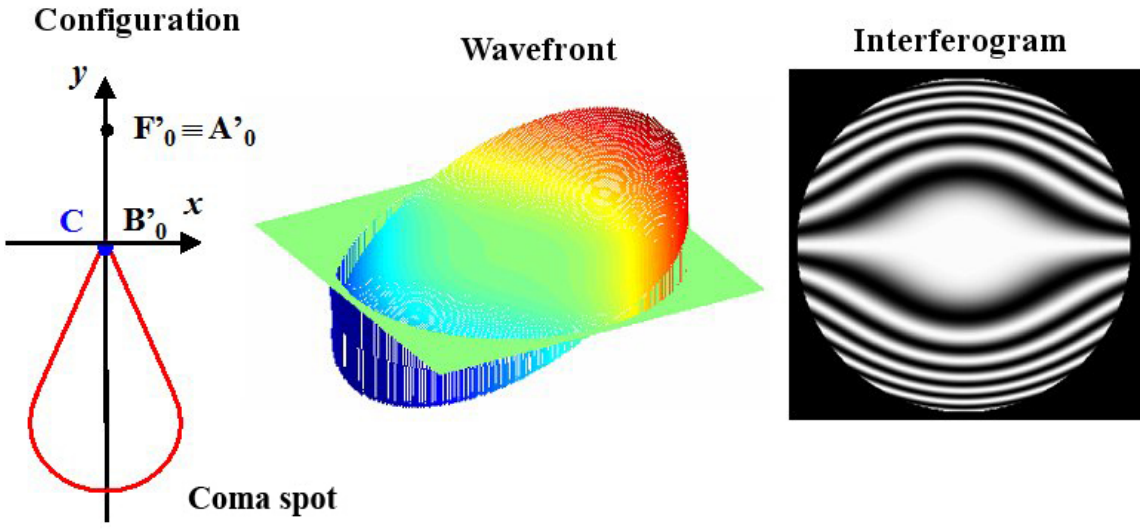

With a tilting of M_2 to put C out of the coma spot, the aberration wavefront becomes:

$$\Delta_O(x,y) = -b_1 y' \frac{y\left(x^2+y^2\right)}{p'^3} - \sin(\alpha_y)\, y$$

Figure 31 illustrates this case.

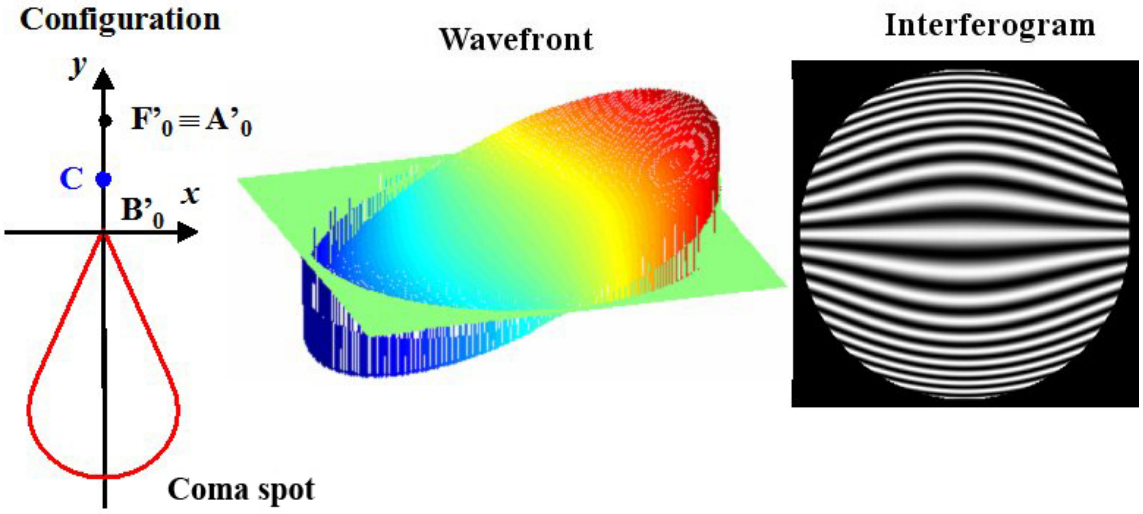

Figure 32 shows the aberration and the interferogram obtained when C is inside the coma spot.

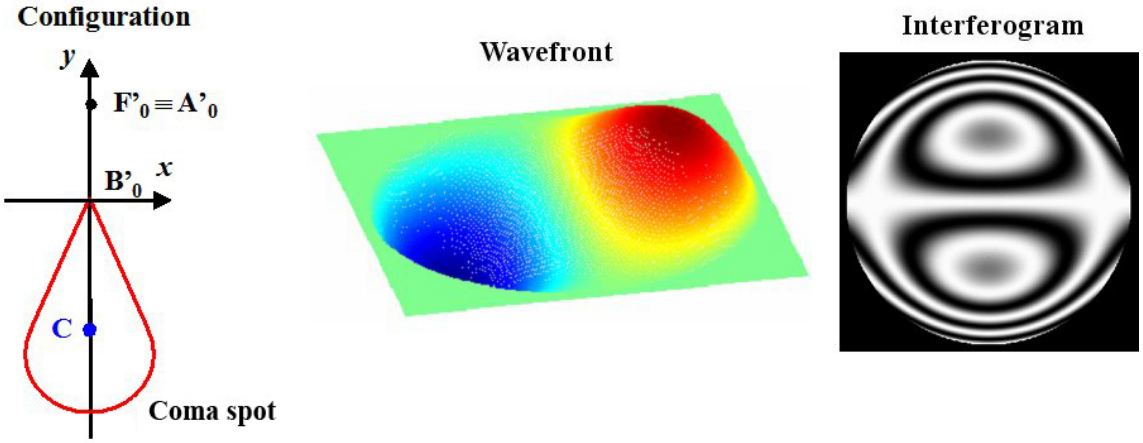

Figure 33 shows the standard deviation and the interferogram obtained when C is moved outside of the meridian plan and outside of the coma spot.

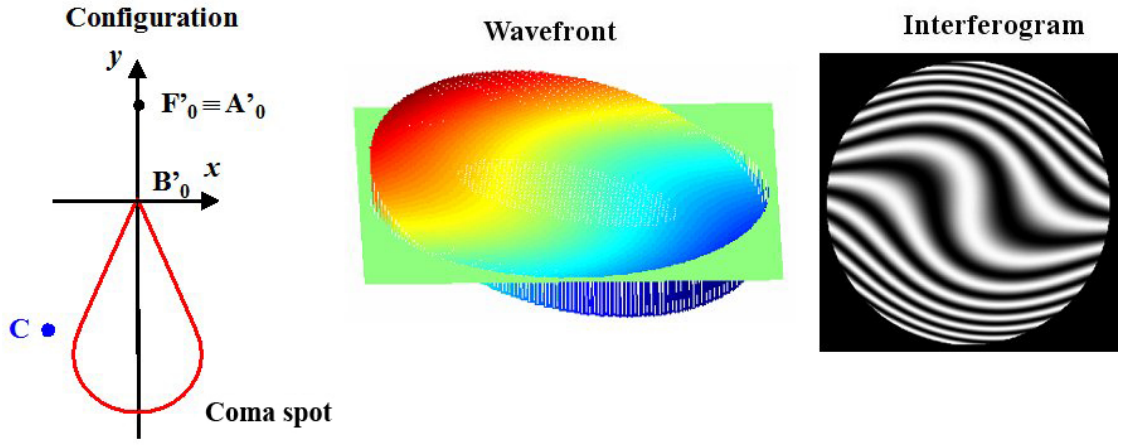

1.7. Interferogram with third-order astigmatism aberration

The astigmatism aberration is also a **field and aperture aberration** that is to say it appears outside the axis for the point. The astigmatism is expressed by the following relation [4 [[4]].5 [[5]]]:

$$\Delta_O(x,y) = -\frac{1}{2p'^2}\left(x^2 t' + y^2 s'\right)$$

Where t' and s' are the tangential and sagittal focal positions related to the paraxial focal planes.

Figure 34 illustrates the wavefront shape and the interferogram with third-order astigmatism when the mirror curvature center is confounded with paraxial image B'_0.

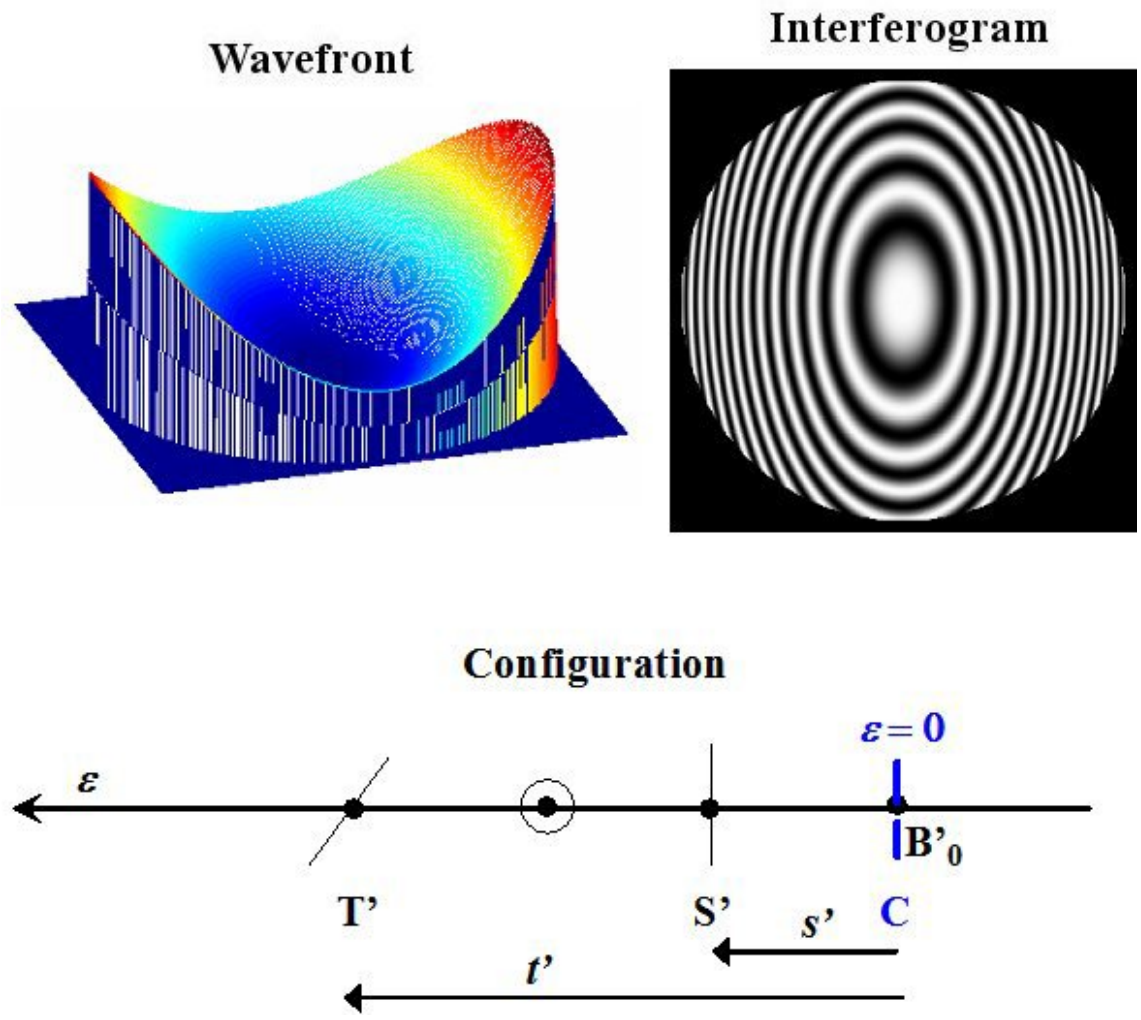

In the case where we defocus spherical mirror M_2, the standard deviation becomes

$$\Delta_O(x,y) = -\frac{1}{2p'^2}\left(x^2(t'-\epsilon) + y^2(s'-\epsilon)\right)$$

For $\varepsilon < 0$, the curvature center is beyond the paraxial image, the wave surface is toric and the fringes are elliptic as illustrated in Figure 35:

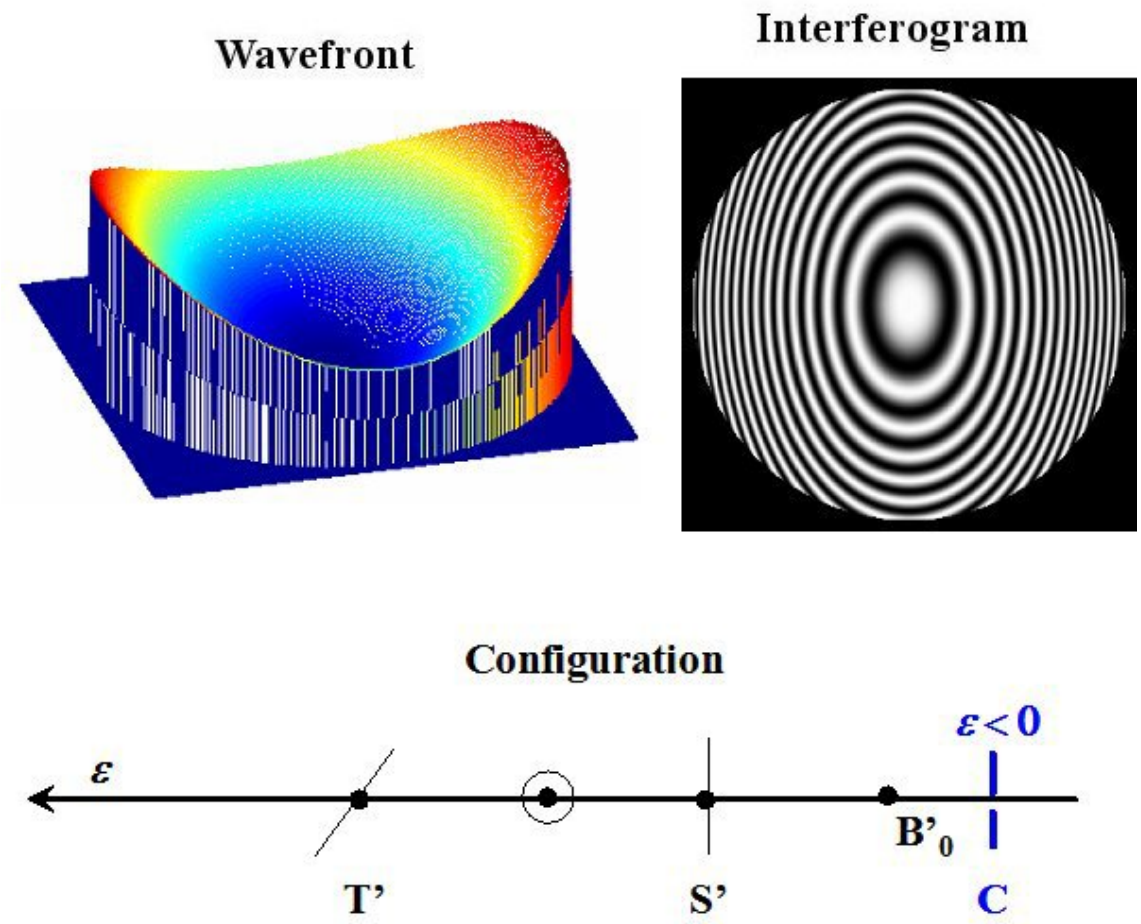

When $\epsilon = s'$, the wave surface is cylinder-shaped with a vertical axis and the fringes are rectilinear and vertical, mirror M_2 curvature center is on the sagittal focus (Figure 36).

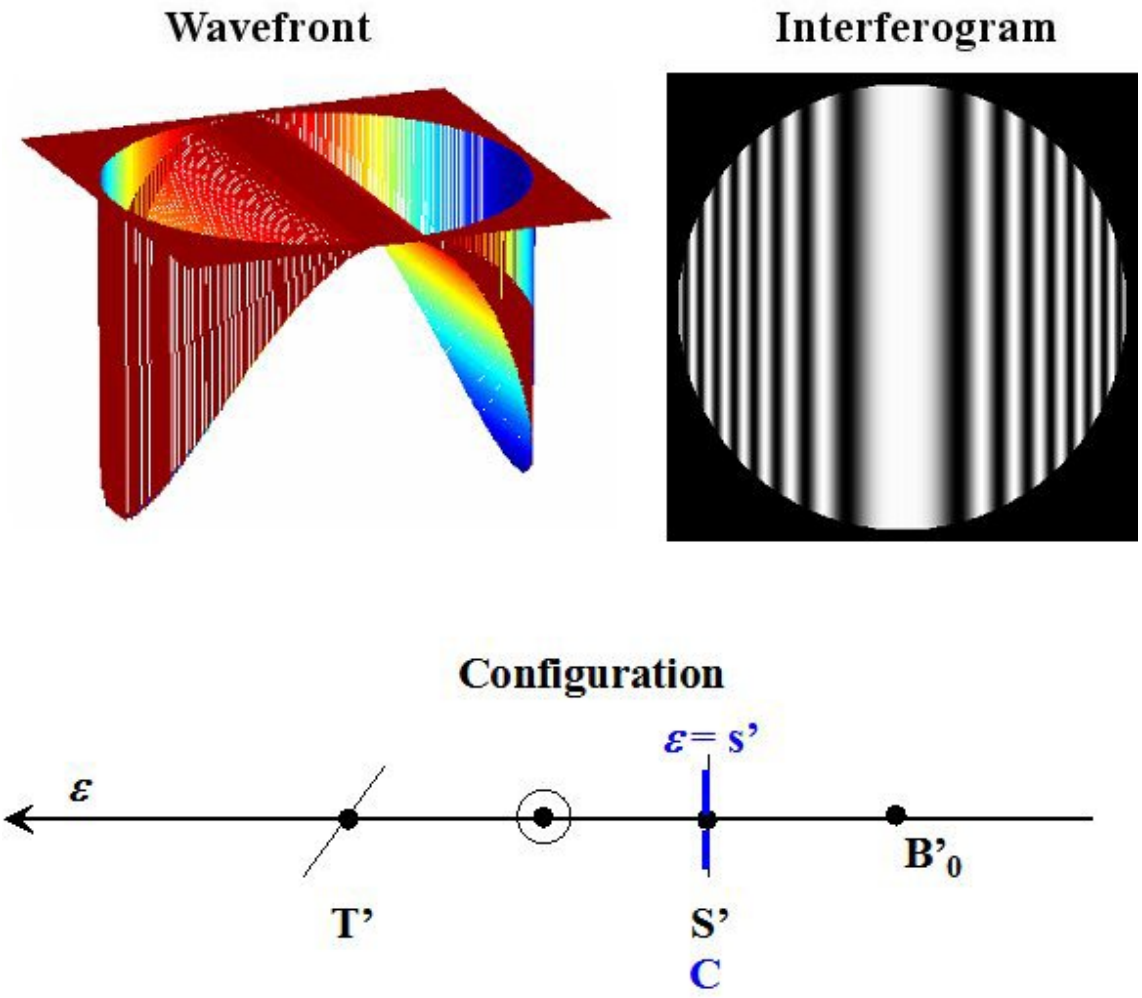

When $\epsilon = (s' + t')/2$, the wavefront surface is diabolo-like torus and the fringes are in the shape of crosses, then mirror M_2 curvature center is localized half way between sagittal and tangential focusal points (Figure 37).

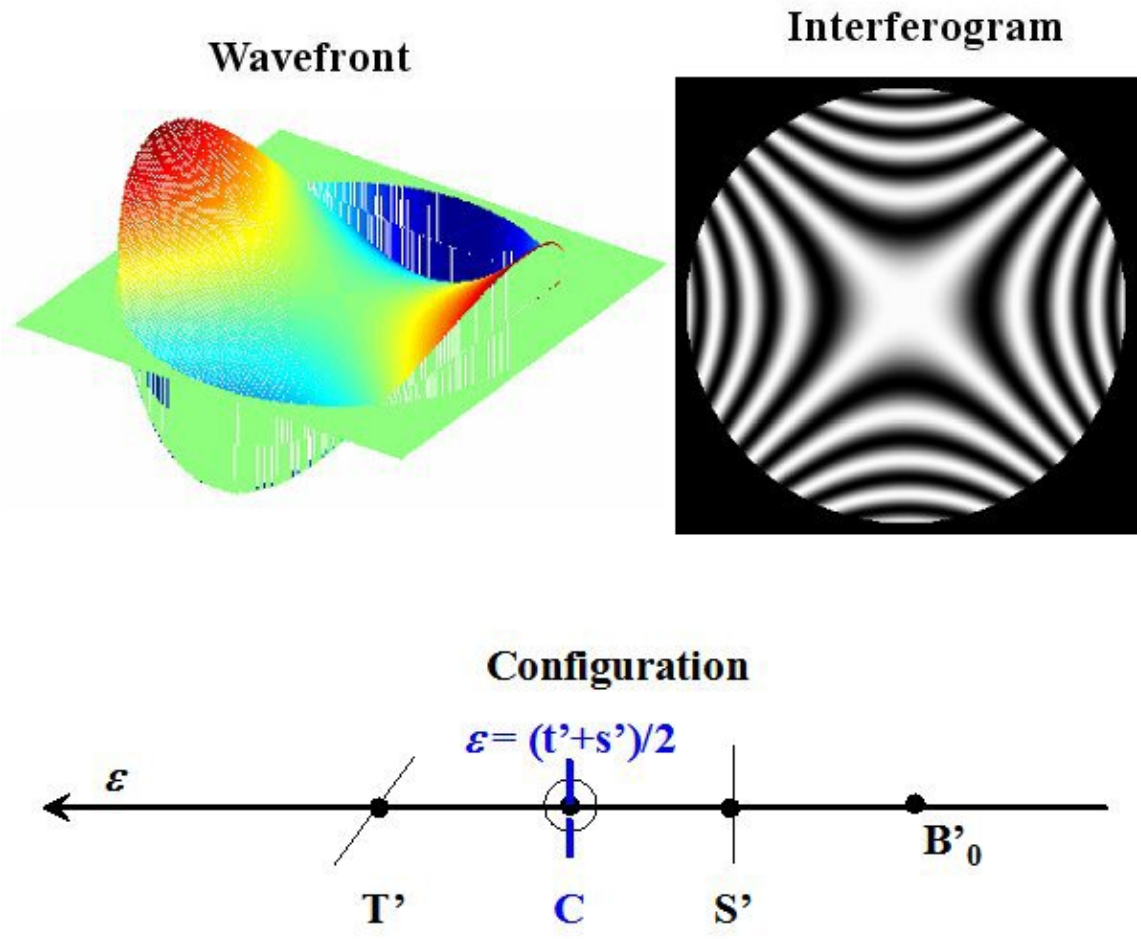

When $\epsilon = t'$, the wavefront surface is cylinder-like again but with an horizontal axis and the fringes are rectilinear and horizontal, then the mirror M_2 curvature center is on the tangential focus (Figure 38).

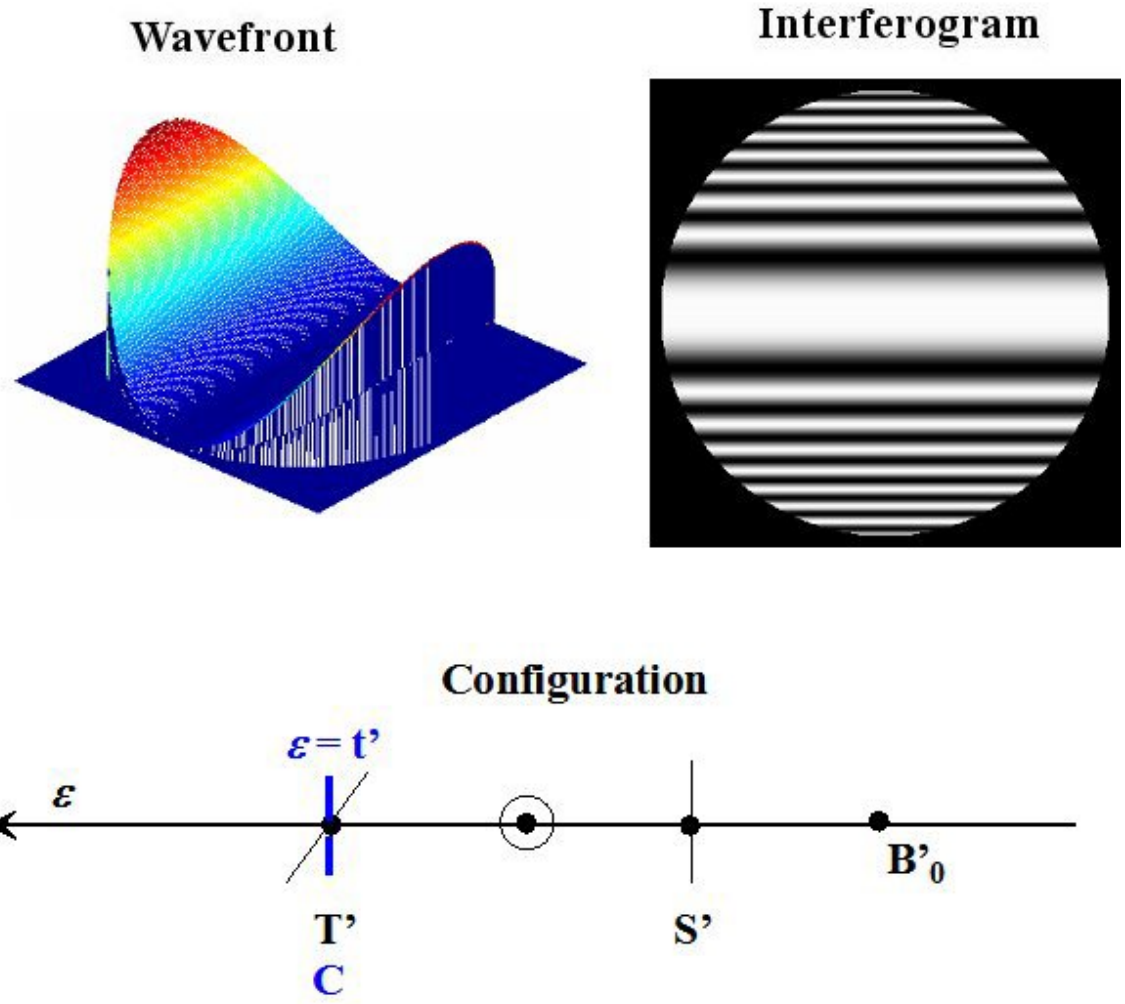

Then, when $\epsilon > t'$, the mirror curvature center is located between the optical system and the tangential focus, the wave surface is toric again and the fringes are elliptical with a horizontal axis (figure 39).

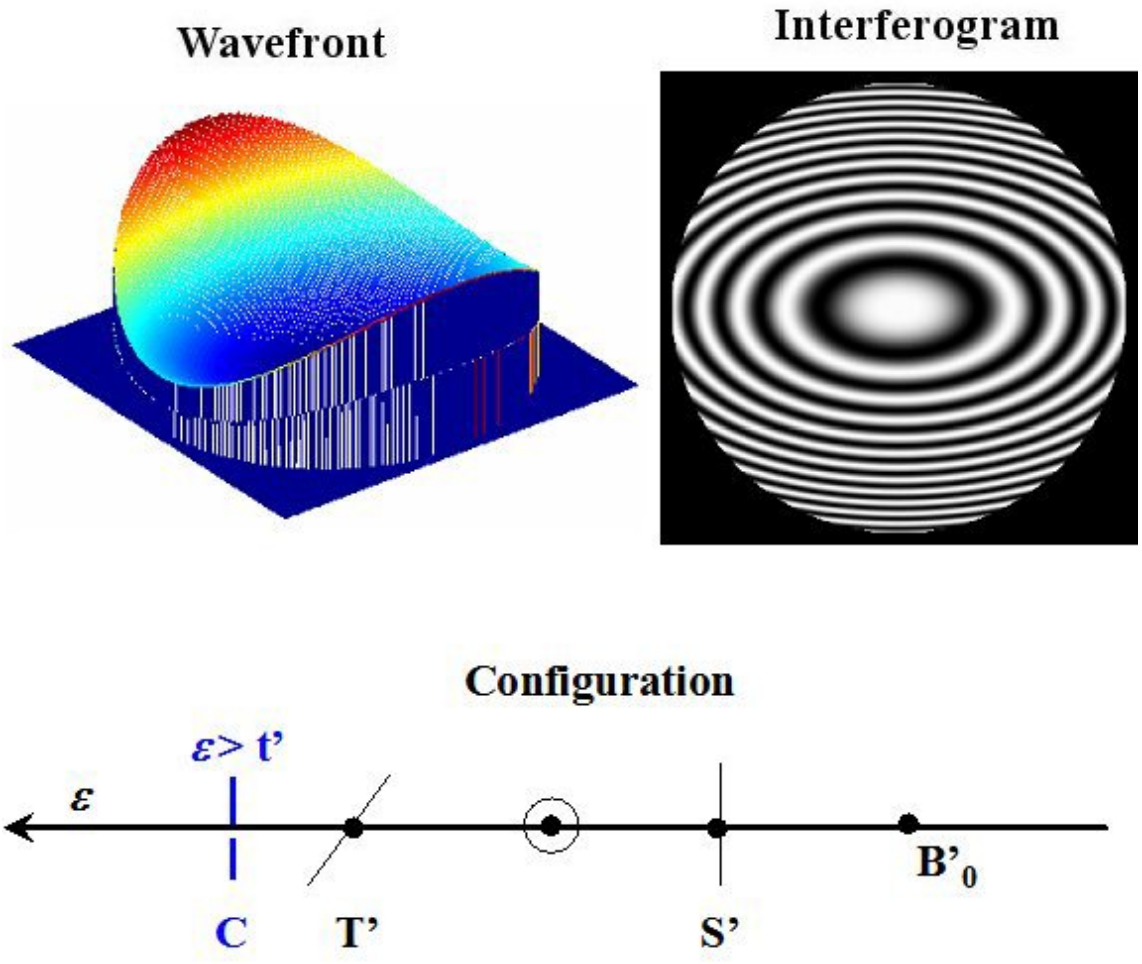

2. Spectrometry by Fourier transform

Fourier transform spectroscopy is one of the interferometer uses. The spectrometry is related to the radiation spectrum measurement. As we have observed before in "**Interferences: Fundamentals**", the light source coherence, thus its spectrum, has a major influence on the interferogram when we modify the optical path difference. Fourier transform spectrometry is a direct application of Wiener-Kinchine theorem. According to "**Interferences: Fundamentals**", the interferogram is written:

$$I(\delta)=a\Re\left[\widetilde{S}_S(0)\right]+b\Re\left[\widetilde{S}_S(\delta)\right]$$

where $\widetilde{S}_S(\delta)$ is the Fourier transform of source energy spectral density, $S_S(\sigma)$, and $\widetilde{S}_S(0)$ its value $\widetilde{S}_S(\delta)$ for $\delta = 0$.

It is also possible to write the interferogram as:

$$I(\delta)=A+\frac{b}{2}\widetilde{S}_S(\delta)+\frac{b}{2}\widetilde{S}_S^*(\delta)$$

The inverse Fourier transform of $I(\delta)$ is:

$$TF^{-1}\left[I(\delta)\right](\sigma)=\int_{-\infty}^{+\infty} I(\delta)\exp\left(2i\pi\delta\sigma\right)d\delta=A\delta(\sigma)+\frac{b}{2}S_S(\sigma)+\frac{b}{2}S_S(-\sigma)$$

Fourier transform is a trimodal function where $\sigma > 0$ part is proportional to the source spectrum. We are used to record the interferogram on a total path difference δ_{max} and the signal is digitalized on N sampling data points. Then we calculate the spectrum with a discrete Fourier transform (FFT algorithm). With this technique, the spectral resolution depends on the discrete Fourier transform filtering function.

Remarque

Let us write this function $\tilde{W}_N(\sigma)$, we have [6 [[6]]]:

$$\left|\tilde{W}_N(\sigma)\right|=\left|\frac{\sin\left(\pi\delta_{\max}\sigma\right)}{\sin\left(\pi\delta_{\max}\sigma/N\right)}\right|\simeq N\left|\mathrm{sinc}\left(\pi\delta_{\max}\sigma\right)\right|$$

Function $\tilde{W}_N(\sigma)$ is the impulse response in the spectrum calculated by FFT. Its width is given by $\Delta\sigma = 1/\delta_{max}$. Thus the spectrometer resolution is given by

$$R_0=\frac{\sigma}{\Delta\sigma}=\sigma\,\delta_{\max}=\frac{\delta_{\max}}{\lambda}$$

Complément

Therefore the resolution depends on the relation between the recorded optical path difference and the average wavelength of the source: it is equal to the number of recorded fringes.

An experimental device explaining this technique is described on Figure 40.

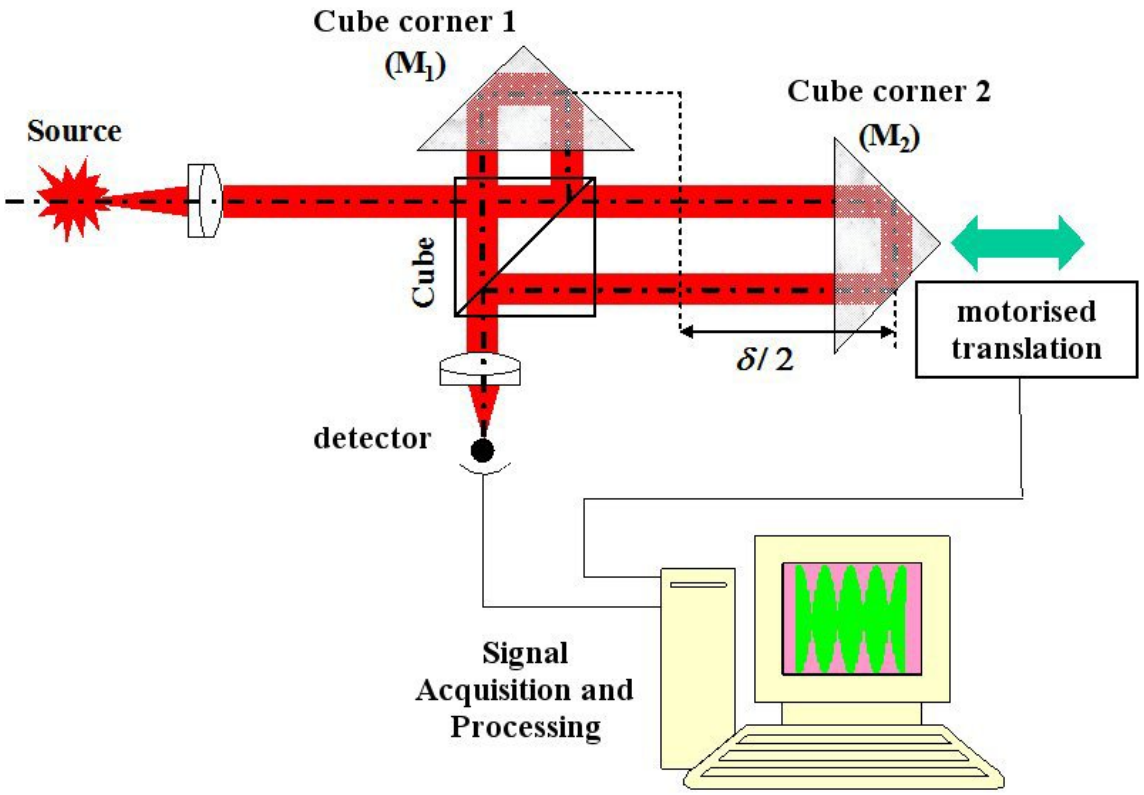

Michelson classical plane mirrors are replaced by two cube corner cubes that have the particularity to reflect the light in the opposite direction. Corner n° 2 is assembled on a computer driven translation stage. For a $\delta/2$ cube movement, we make a δ optical path difference. Thanks to the corner cubes used there is no need to realign the mirror-cube after each translation. The signal acquisition by the detector is computer driven in a synchronic way with the cube translation.

As an illustration, Figure 41 shows the interferogram obtained with a sodium based low pressure lamp.

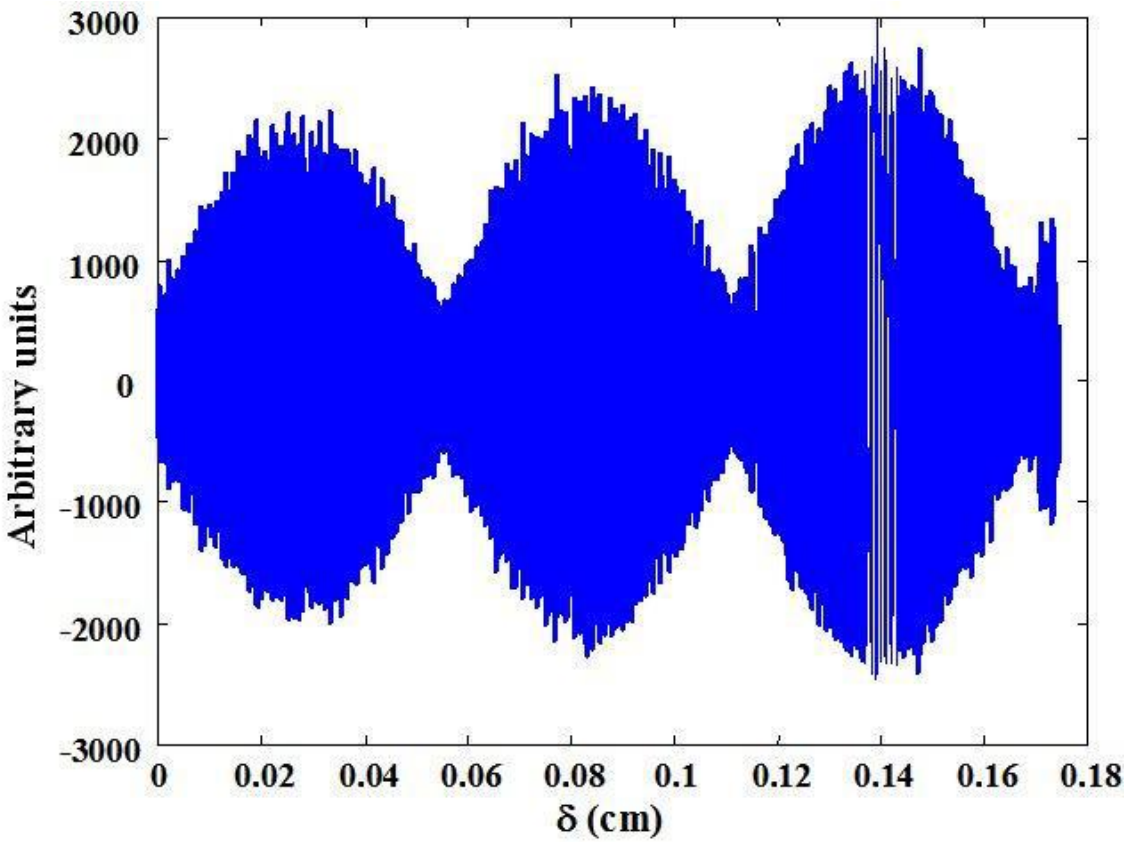

The FFT calculation gives Figure 42 results. We can observe the spectrum symmetry.

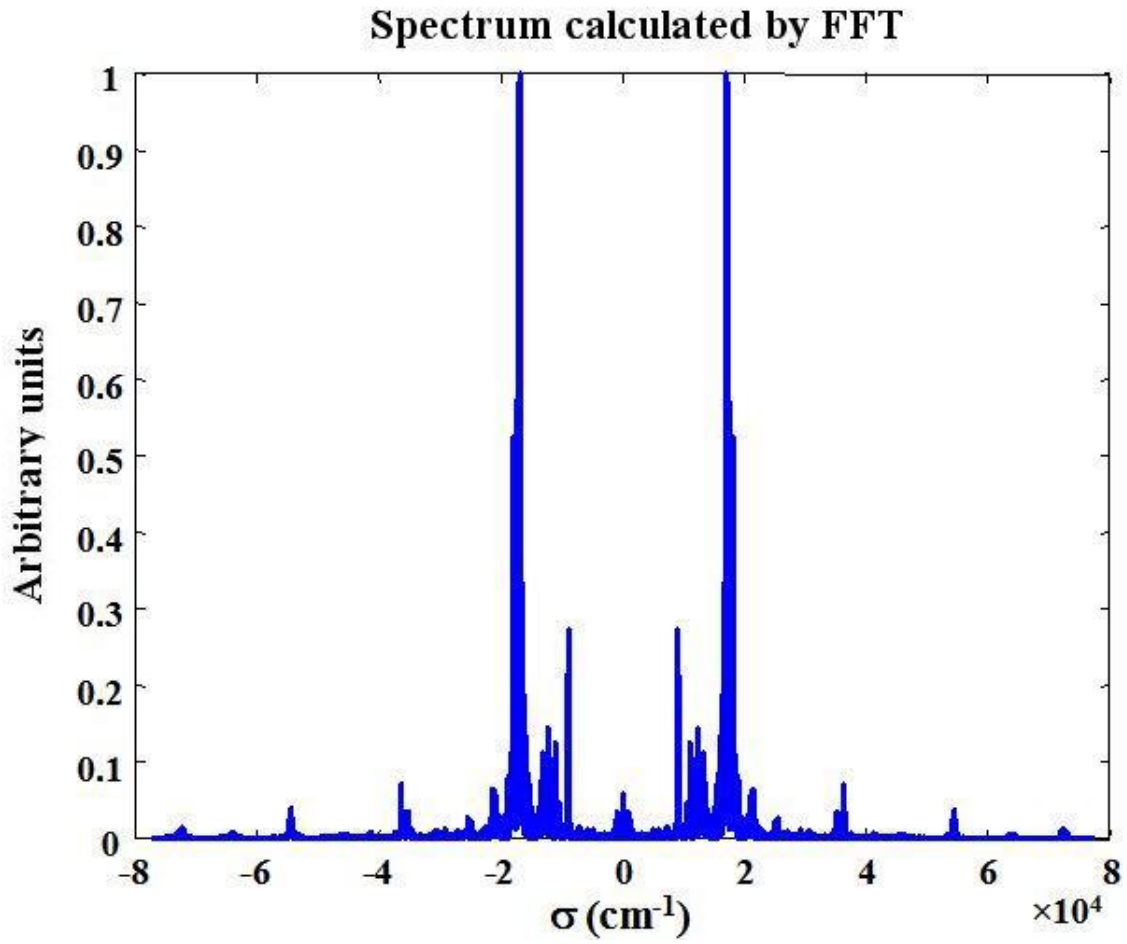

After the extraction of the positive wave number part, the source spectrum as a function of the wavelength is given in Figure 43.

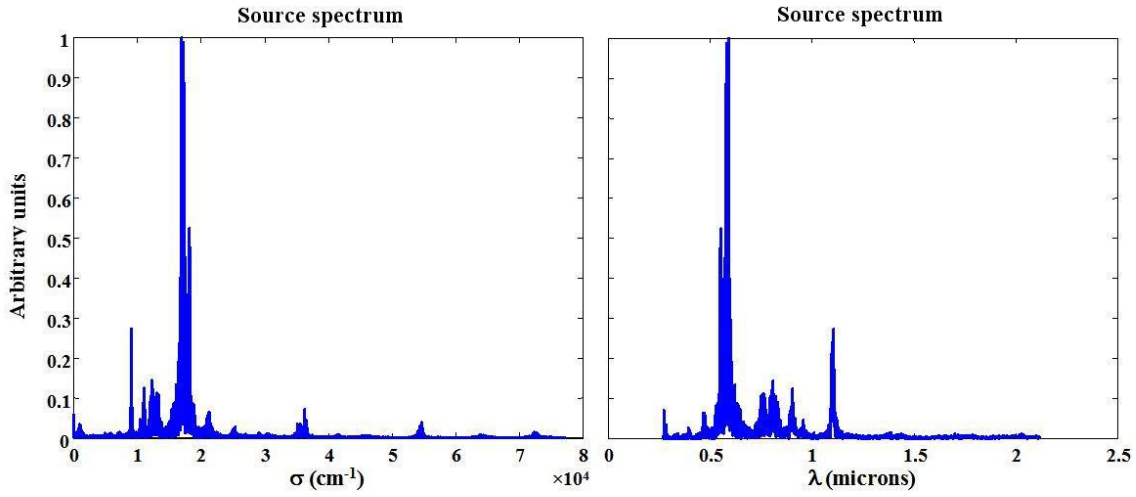

There is a second illustration, with an incandescent lamp, whose measured interferogram is given in Figure 44.

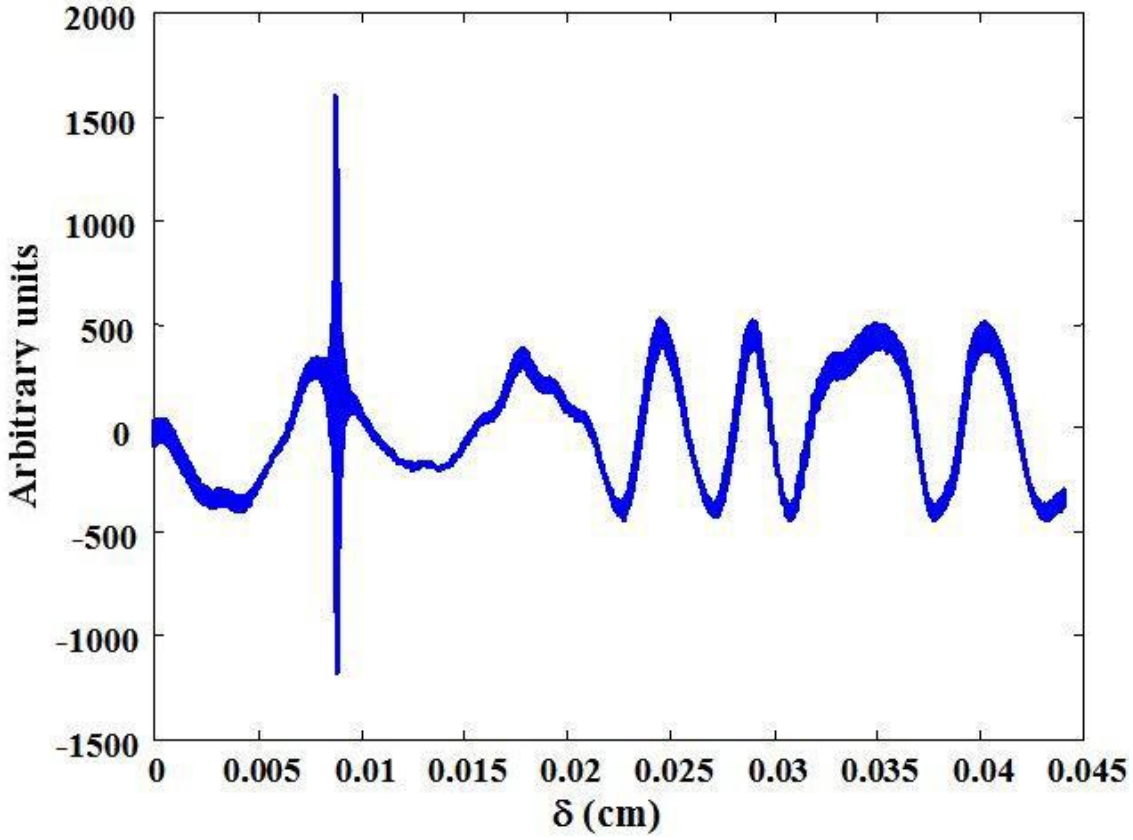

After computing, the source spectrum as a function of the wavelength is represented on figure 45.

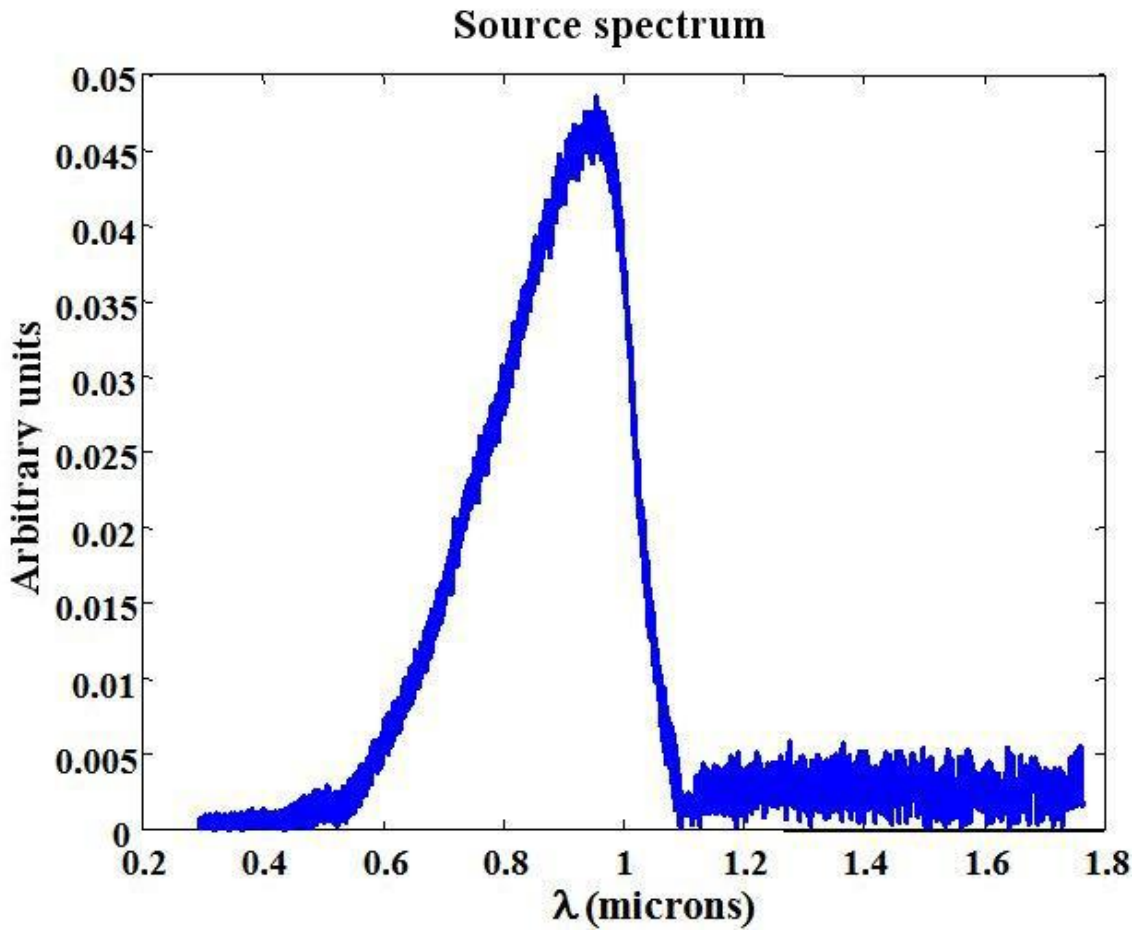

The later result needs a comment about the spectrum observation as a function of the wavelength. The incandescent lamp is a black field-type source whose spectral band is very wide and covers from the UV ray to the IR. But the Figure 45 result shows that the spectrum is strongly decreasing around $1,1\ \mu\mathrm{m}$. That is due to the sensitivity spectral band of the detector that cuts at that wavelength and that is used in the Figure 40 device. It is due to the infrared filter of the detector. Thus we can observe that the measured spectrum is influenced by the sensor spectrum sensitivity. It is important to correct the measurement and to process the spectrum dividing it by the sensor sensitivity for all the measurable wavelengths. This process has not been applied for the results shown in that example.

3. Fabry-Perot spectrometry

Fabry-Perot multiple beam interferometer can be used as a spectrometer. The experimental configuration is described in Figure 46. It is **confocal** Fabry-Perot: the mirrors are spherical with the same curvature and their focal points are confounded, the cavity is stable so that the light can go back and forth to infinity staying localized around the optical axis.

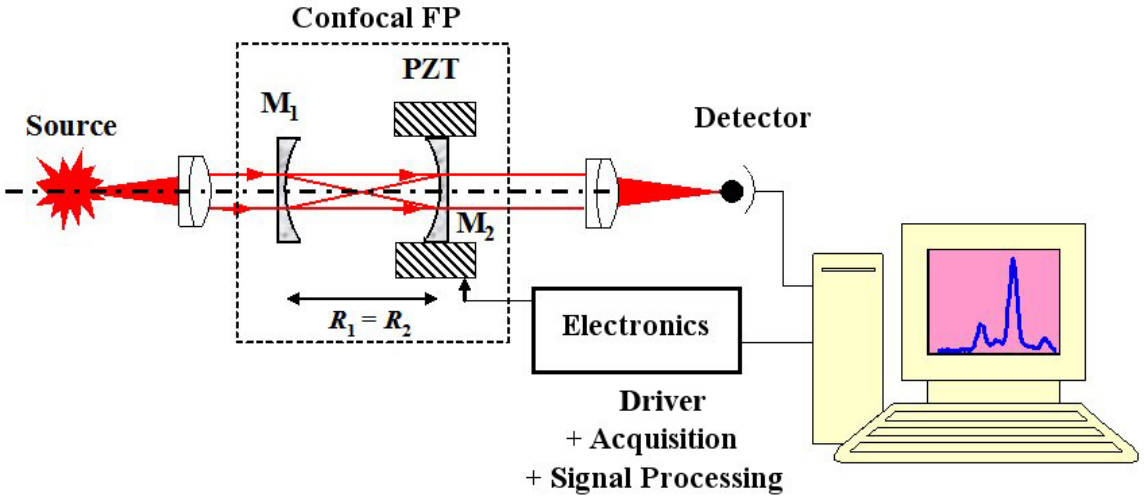

One of the mirrors is assembled on a piezoelectric transducer in order to make the cavity thickness varying and to do a spectral scanning. The PZT driver voltage is a ramp. For each spectrum frequency which is in phase with the cavity length, the signal on the detector is maximal.

As an illustration, Figure 47 outlines the principle in the case of a multimode HeNe laser. Figure 47b shows the tension ramp that drives the PZT and we can observe the laser spectrum in Figure 47a.

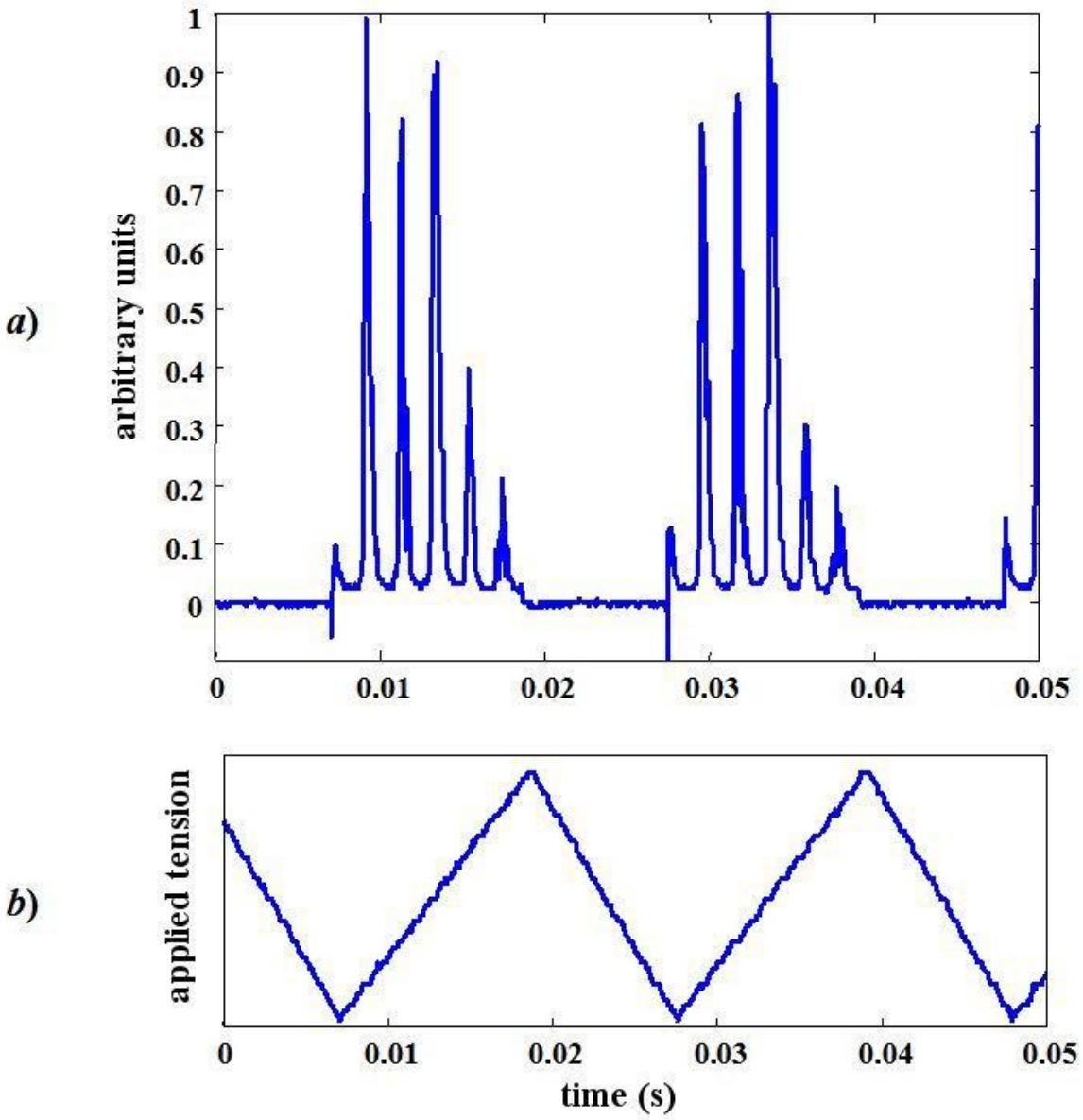

Figure 48 corresponds to a signal period observed in Figure 47a. The horizontal axis is given in wave number by correspondence between the scale of frequency and the temporal one. Indeed, a period signal of Figure 47 corresponds to the Fabry-Perot free spectral interval.

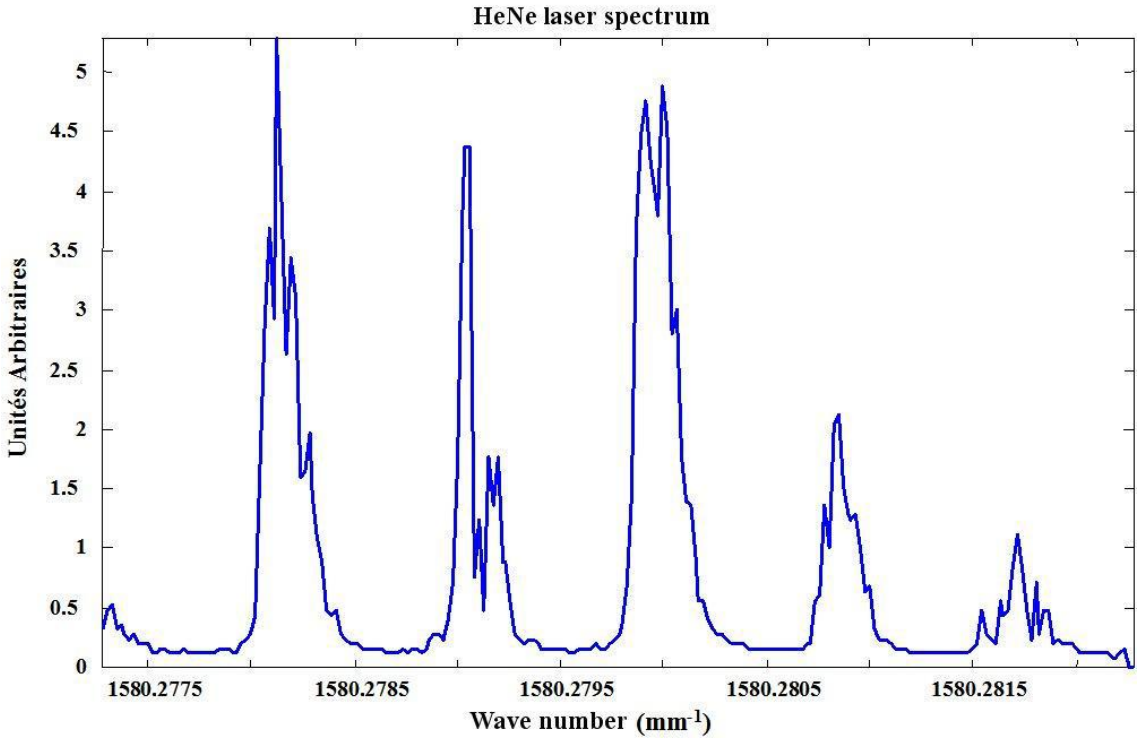

The characteristics of that spectrometer are the following:

- Free spectral range $\Delta\nu = 1,5\ \text{GHz}$ namely $\Delta\sigma = 0,005\ \text{mm}^{-1}$
- Thinness $F = 200$
- Instrumental resolution $\delta\nu = 7,5\ \text{MHz}$ namely $\delta\sigma = 2,5 \times 10^{-5}\text{mm}^{-1}$
- Digital sampling $\delta\nu = 6,72\ \text{MHz}$ namely $\delta\sigma = 2,24 \times 10^{-5}\text{mm}^{-1}$

As the air cavity thickness made by both mirrors is $ne = R_1$,the spectrometer resolution is given by (see Figure 18 for the notes):

$$R_0 = \frac{\sigma}{\delta\sigma} = \frac{\sigma}{\Delta\sigma} F = \frac{2R_1}{\lambda} F$$

It is proportional to the interferometer thickness and depends on the average wavelength.

Attention

It is possible to calculate the degree of coherence as well as the coherence length from the spectrum measurement.

According to "**Interferences: Fundamentals**", the degree of coherence is given by:

$$\gamma_{c,t}(\delta) = \Re\left[\frac{\widetilde{S}_0(\delta)}{\widetilde{S}_0(0)}\right]$$

Where $\tilde{S}_0(\delta)$ is the Fourier transform $S_0(\sigma)$, radiation spectral envelop.

The coherence length can be estimated by:

$$l_c = \int_{-\infty}^{+\infty} |\gamma_{c,t}(\delta)|^2 d\,\delta$$

Considering that the Fabry Perot spectrum measurement gives quantity $S_0(\sigma)$, the degree of coherence is calculated by a discret Fourier transform of the measured spectrum. Figure 49 shows laser HeNe degree of coherence calculated from result of Figure 48.

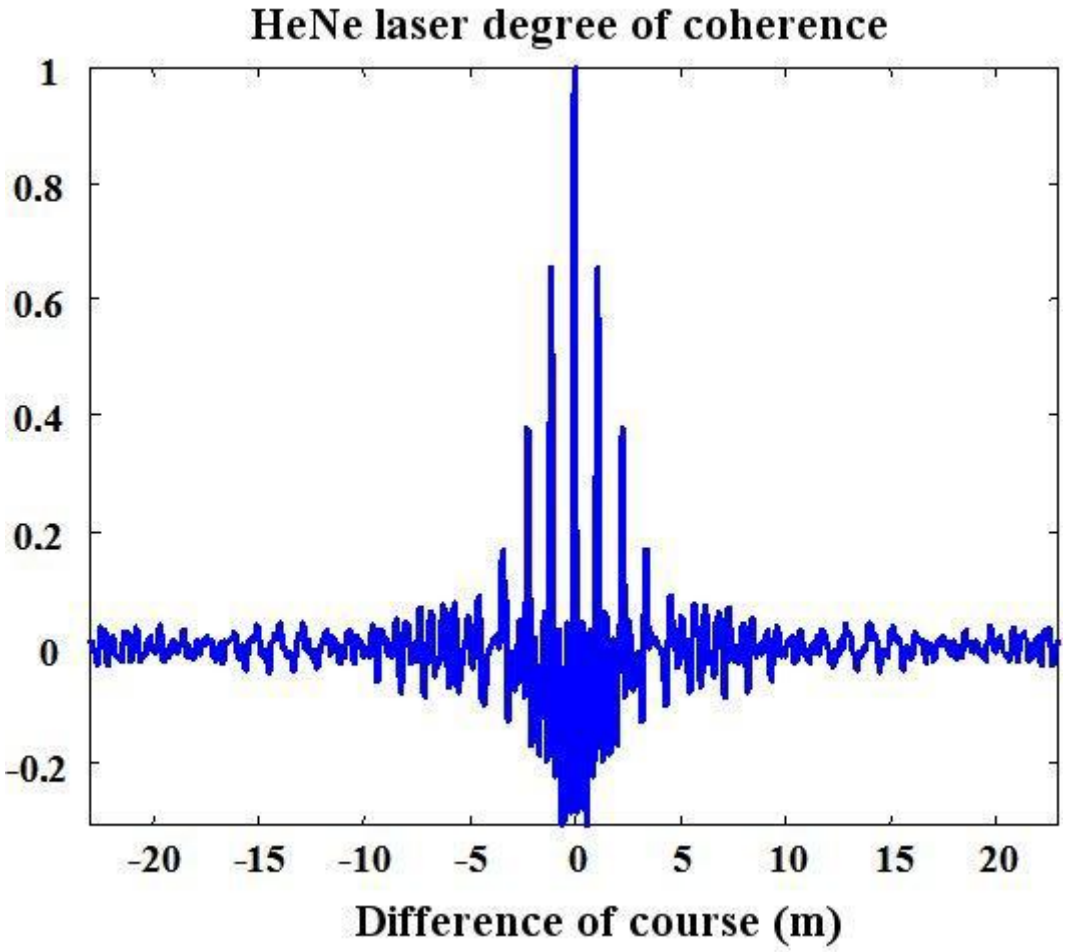

The coherence length computed with the degree of coherence is estimated as to be $l_c \approx 33,7 \text{ cm}$.

Another illustration is about a laser diode at $\lambda = 661 \text{ nm}$ which is measured by the interferometer as illustrated in Figure 50.

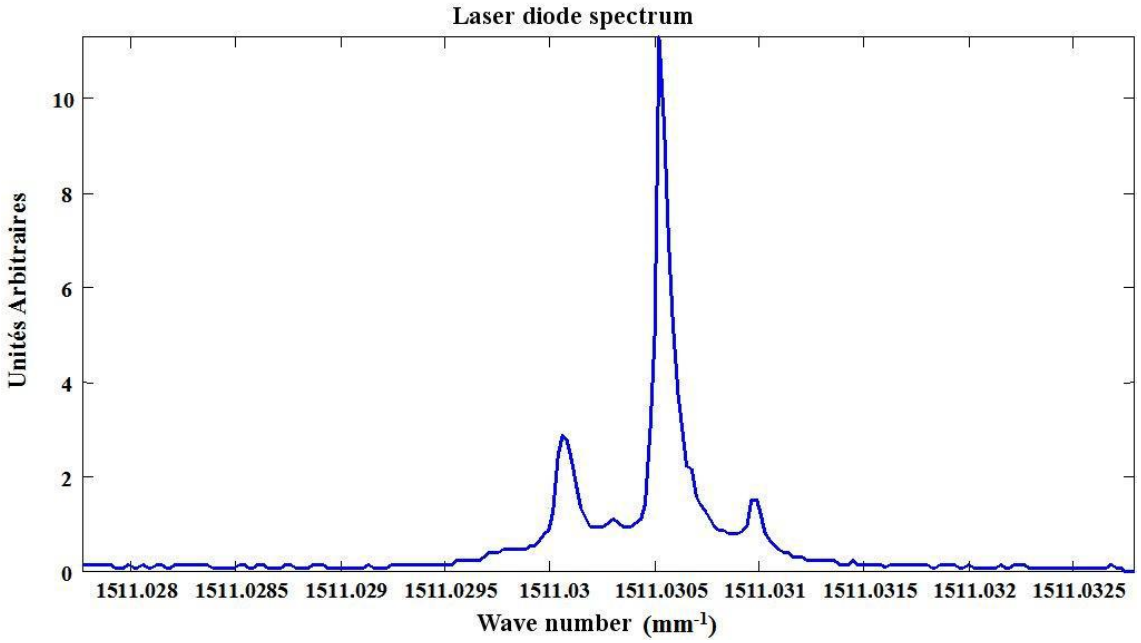

The laser diode degree of coherence is calculated by FFT and is represented in Figure 51. Its coherence length is estimated as equal to $l_c \approx 58,1$ cm.

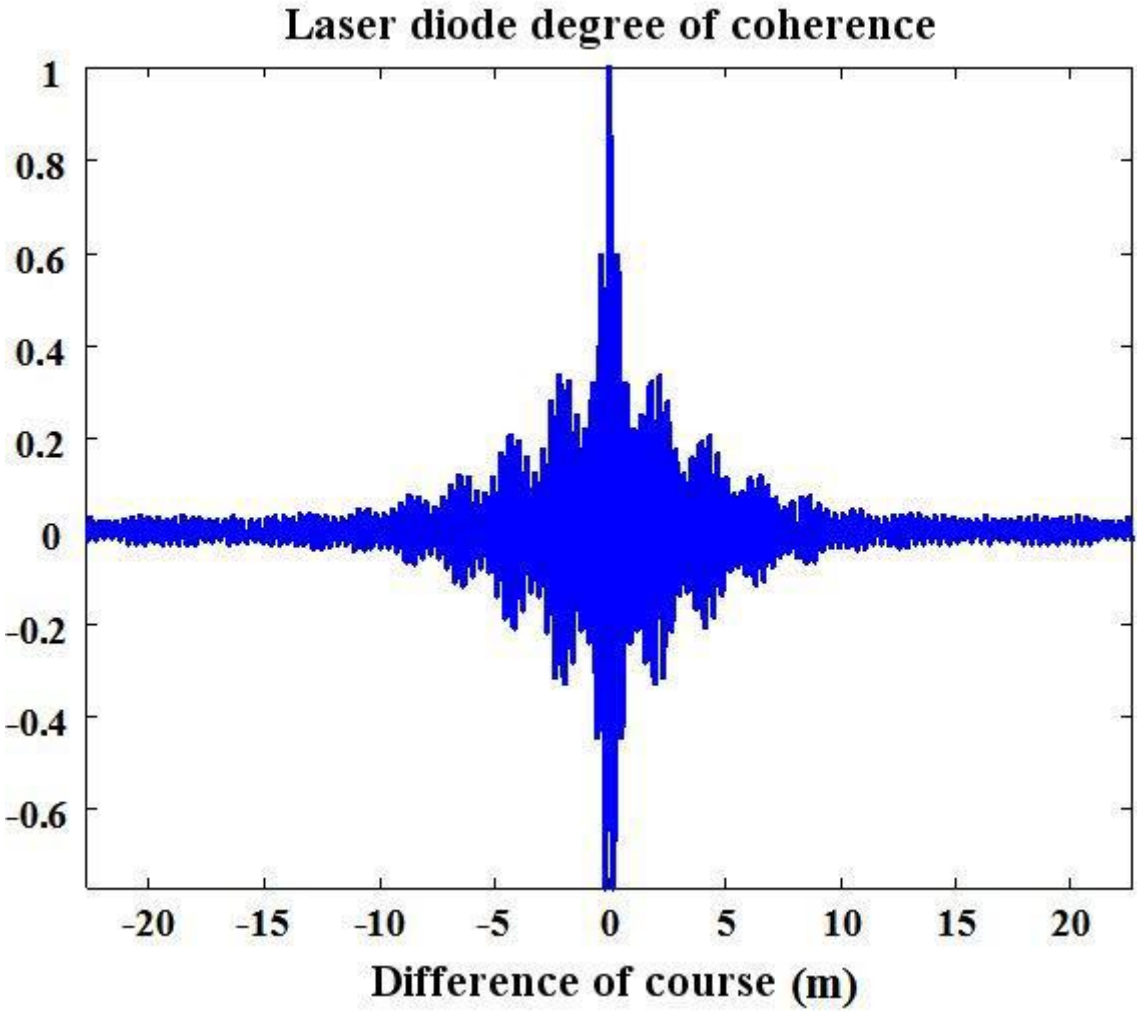
Laser diode degree of coherence
1
0.8
0.6
0.4
0.2
0
-0.2
-0.4
-0.6
-20
-15
-10
-5
0
5
10
15
20
Difference of course (m)

IV.Exercices

1. Question 1 : Fill in the gaps

Question

[Solution n°1 p 60]

Complete this text with the words given in Table 1

Finally, the interference phenomenon is quite simple, its origin is due to one physical parameter which is the, ... and which represents the . . . . . between two paths along which the light is propagating. In the case of two wave interferences with a perfect coherence of the source, the intensity is . . . (give a mathematical relation) . . . . A perfectly coherent wave is a light having temporal coherence, this means that the source is . . . . . ,it is also a spatially coherent source meaning that the source is . . . . . If the light is not coherent, the . . . . . is decreased and the normalized intensity can be written in the form of . . . (give a mathematical relation) . . . . There exists two types of interferometers, the ones are said to be . . . . . -splitting as . . . . . and the other ones are said to be . . . . . -splitting as . . . . . . The advantage of . . . . . -splitting interferometers compared to the other ones is their luminosity. In the case of an extended source, if interferences exist, they are . . . . . With the Michelson interferometer there exist two types of set-ups: that said as . . . . . plate for which interferences are localized at infinity and that said as . . . . . for which interferences are localized . . . . . For a bright fringe, the . . . . . is equal to an integer number times the wavelength; for a dark fringe it is equal to an . . . . . .times the . . . . . In the screen, the spatial period is called . . . . . .

Here is a list of words you may use. A word can be used several times or other never.

Michelson interferometer	Fabry-Perot interferometer
Young slits	monochromatic
polychromatic	air plate
air corner	amplitude
wavefront	interfringe
on the mirrors	infinity
parallel face	wavefront
wave surface	optical path difference
path difference	even integer number
odd integer number	integer number
wavelength	half-wavelength
quarter-wavelength	localized
non localized	coherent
incoherent	large
punctual	contrast
parallel beam	corner plate

2. Question 2 : Principle of a laser velocimeter

Two monochromatic plane waves that passed through the same optical path and issued from the same laser interfere in a laminar flow of a liquid. Wave vectors $\vec{k_1}$ and $\vec{k_2}$ of both waves do 2θ angle. The liquid flow is perpendicular to vector $\vec{k} = \vec{k_1} + \vec{k_2}$ directed in the x axis. Figure 52 illustrates the principle of the velocimeter.

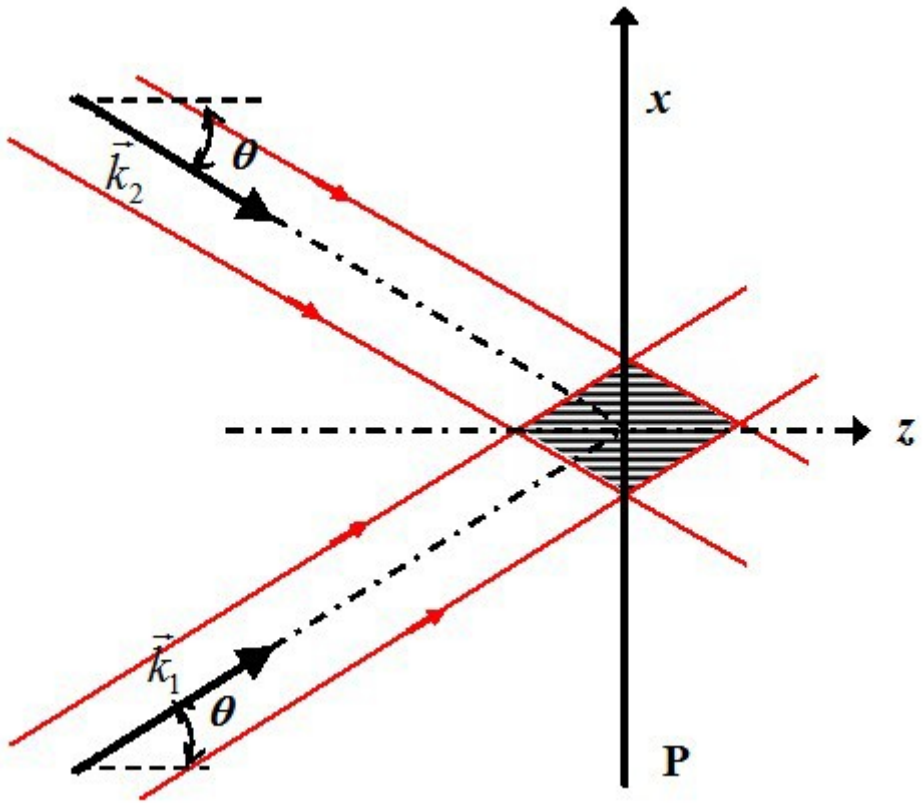

A diffusing particle M of about $0.5\ \mu\mathrm{m}$ in diameter, included in the flow crosses the interference field and diffuses light only when it is in a bright fringe. A photodetector detects the light diffused by the particle and gives an electrical signal which frequency f_0 depends on the particle velocity V_x.

Question

[*Solution n°2 p 60*]

a) Find the intensity distribution in plane P, describe the fringes aspect and calculate the interfringe.

b) Find the expression of fluid flow velocity V_x assuming that the particle perfectly follows the flow.

3. Question 3 : Velocity measurement

Refraction index n of the flow medium is 1,33. The laser is a continuous ionized argon laser which main wavelengths are, in term of power, $514,5\ \mathrm{nm}$, $496,5\ \mathrm{nm}$, $488,0\ \mathrm{nm}$, and $476,5\ \mathrm{nm}$. The wavelength beam $\lambda_0 = 514.5\ \mathrm{nm}$ is selected. The laser beam has diameter $D_1 = 1.5\ \mathrm{mm}$, is divided into two parallel and same intensity beams with no path difference at the output of the wavefront-splitter. Each beam is distant from the other one of $\Delta x = 3\ \mathrm{cm}$. A focusing lens with a focal length $f' = 500\ \mathrm{mm}$ make the beams converge in its image focal point F'. At this point, the measurement volume (V) has a diameter Φ which value depends on the wavelength, on f' and on diameter D_1. We have:

$$\Phi = \frac{4\,\lambda_0\,f'}{\pi\,n\,D_1}$$

The detector detects a $20\ \mathrm{MHz}$ frequency. Figure 53 gives the experimental configuration.

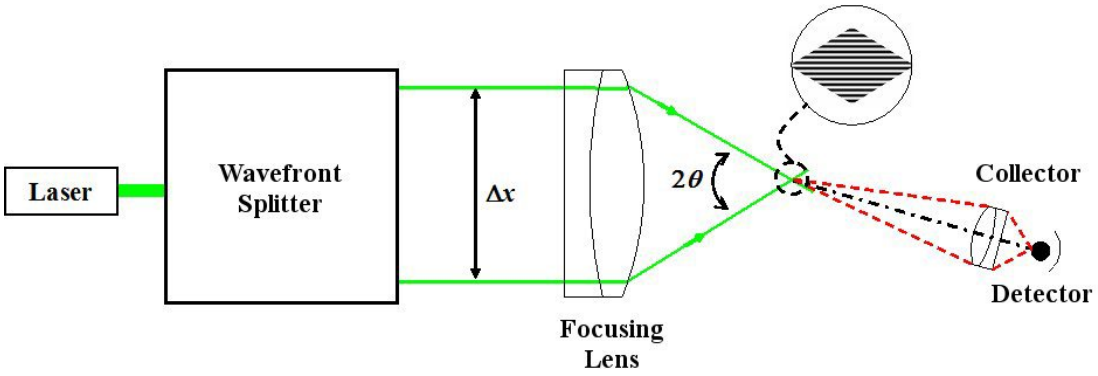

Question

[Solution n°3 p 61]

Deduce of these experimental conditions:

a) Angle θ

b) Interfringe i

c) Measurement volume diameter Φ

d) Fluid velocity V_x

Remarks :

1. The set-up described above does not make it possible to determine the velocity direction. In the exercise, the direction was to be known. If it is not the case, in order to find this out, we make the fringes beating. This is done by putting a Bragg cell (acousto optic modulaton) in one of the arm of the interferometer.
2. Using the different line of laser emission in the same measurement volume, three interferences fringes networks of different colors can be obtained and so make it possible to detect the three components of an unknown velocity direction.
3. The adjustment of the beam convergence must be done carefully so that the beams intersection is located at the waist to obtain flat, equidistant and well contrasted fringes (figure 54). In that case only, the measured frequency will not depend on the particle position in the measurement volume.

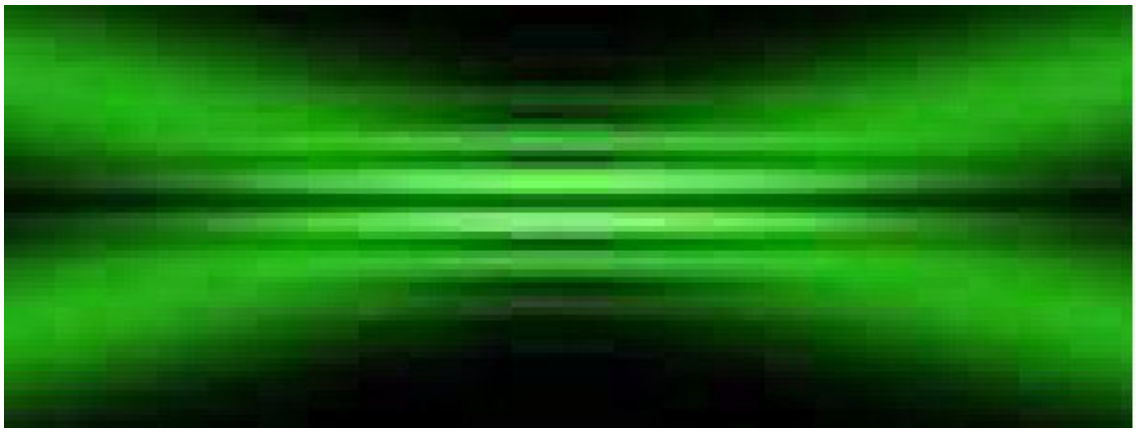

For further information the reader should consult the list of references [7 [[7]].8 [[8]]].

Solution des exercices

>Solution n°1 *(exercice p. 57)*

Finally, the interference phenomenon is quite simple, its origin is due to one physical parameter which is the **path difference**, and which represents the **optical path difference** between two paths along which the light is propagating. In the case of two wave interferences with a perfect coherence of the source, the intensity is $I_0/2(1+\cos(\varphi))$. A perfectly coherent wave is a light having temporal coherence, this means that the source is **monochromatic**, it is also a spatially coherent source meaning that the source is **punctual**. If the light is not coherent, the **contrast** is decreased and the normalized intensity can be written in the form of $I_0/2(1+\gamma\cos(\varphi))$. There exists two types of interferometers, the ones are said to be **wavefront**-splitting as **Young slits** and the other ones are said to be **amplitude**-splitting as **Michelson interferometer**. The advantages of **amplitude**-splitting iinterferometers compared to the other ones is their luminosity. In the case of an extended source, if interferences exist, they are **localized**. With the Michelson interferometer there exist two types of set-ups: that said as **parallel face** plate for which interferences are localized at infinity and that said as **air corner** for which interferences are localized **on the mirrors**. For a bright fringe, the **optical path difference** is equal to an integer number times the wavelength ; for a dark fringe it is equal to an **odd integer number**times the **half-wavelength**. In the screen, the spatial period is called **interfringe**.

>Solution n°2 *(exercice p. 58)*

a) In order to simplify notations, we can choose that the amplitude of the electrical field equals the unity, and that both beams have parallel polarization. For the first wave we have:

$$\vec{E}_1(\vec{r},t)=\exp(-i\omega t)\exp\left(i\vec{k}_1.\vec{r}\right)$$

And:

$$\vec{E}_2(\vec{r},t)=\exp(-i\omega t)\exp\left(i\vec{k}_2.\vec{r}\right)$$

For the second one.
The electromagnetic field is given by the sum of the complex amplitudes, namely:

$$\vec{E}(\vec{r},t)=\vec{E}_1(\vec{r},t)+E_2(\vec{r},t)$$

The intensity on the screen is proportional to the square complex amplitude:

$$I(\vec{r})=1+\cos\left(\left(\vec{k}_1-\vec{k}_2\right).\vec{r}\right)$$

Let us consider that plane P is located in $z=0$, the coordinates of the vector describing the position of a point M in plane P are:

$$\vec{r}=\begin{cases}x\\y\\0\end{cases}$$

In the fluid, the wave vectors of the waves have the same modulus $|\vec{k_1}| = |\vec{k_2}| = \frac{2\pi}{\lambda}$ with $\lambda = \lambda_0/n$, n is the fluid refractive index. The wave vectors are respectively:

$$\vec{k}_1 = \frac{2\pi}{\lambda}\begin{cases}\sin(\theta)\\0\\\cos(\theta)\end{cases} \qquad \vec{k}_2 = \frac{2\pi}{\lambda}\begin{cases}-\sin(\theta)\\0\\\cos(\theta)\end{cases}$$

Vector $\vec{k_1} - \vec{k_2}$ is oriented along x and its coordinates are:

$$\vec{k}_1 - \vec{k}_2 = \frac{4\pi}{\lambda}\begin{cases}\sin(\theta)\\0\\0\end{cases}$$

So the intensity is expressed as:

$$I(\vec{r}) = 1 + \cos\left(\frac{4\pi}{\lambda}\sin(\theta)\,x\right)$$

The location of points having the same intensity corresponds to a succession of planes that are parallel to axis z, of abscissa $x = C^{ste}$ regularly spaced from interfringe i. The expression of the interfringe is:

$$i = \frac{\lambda}{2\sin\theta} = \frac{\lambda_0}{2n\sin\theta}$$

b) If the particle moves at velocity V_x along the x axis, then the time that needs a particle to propagate along the interfringe is $\Delta t = 1/f_0$, so that:

$$V_x = \frac{i}{\Delta t} = i\,f_0 = \frac{\lambda_0 f_0}{2n\sin\theta}$$

>Solution n°3 *(exercice p. 59)*

a) As angle θ is small, we can write (see figure 53):

$$\Delta x \approx 2\theta f'$$

So:

$$\theta = \frac{\Delta n}{2f'} = \frac{3\times10^{-2}}{2\times0.5}$$

Hence $\theta = 3\times10^{-2}$ rad $= 1,72.$

b) The laser wavelength is $\lambda_0 = 514,5$ nm and the interfringe is:

$$i = \frac{\lambda_0}{2n\sin\theta} = \frac{0.5145}{2\times1.33\times3\times10^{-2}} = 6.4\,\text{microns}$$

c) The measurement volume is:

$$\Phi = \frac{4\lambda_0 f'}{\pi n D_1} = \frac{4 \times 0.5145 \times 500}{\pi \times 1.33 \times 1.5} = 164 \text{ microns}$$

d) The fluid velocity is estimated to be:

$$V_x = \frac{\lambda_0 f_0}{2n \sin\theta} = \frac{0.5145 \times 20 \times 10^6}{2 \times 1.33 \times 3 \times 10^{-2}} = 129 \text{ m/s}$$

Bibliographie

[[1]] Joelle Surrel, *Optique Instrumentale et Optique de Fourier*, Éditions Ellipse, Paris, 1996.

[[2]] J.C. Radix, *Gyromètres optiques*, Les Techniques de l'Ingénieur, R1945, Paris, 1999.

[[3]] A. Maurel, *Optique Ondulatoire*, Editions Belin, Paris, 2003.

[[4]] Daniel Malacara, *Optical shop testing*, Éditions Wiley Interscience, New York, 1992, 2ème Édition.

[[5]] Max Born, Emil Wolf, *Principle of Optics, 7ème Edition*, Cambridge University Press, Cambridge, 1999.

[[6]] Jacques Max, Jean Louis Lacoume, *Méthodes et Techniques de Traitement du Signal et Application aux Mesures Physiques, Tome 1 - Principes Généraux et Méthodes Classiques*, Editions Masson, Paris, 1996.

[[7]] M. Philbert, A. Boutier, *Visualisation et procédés optiques de mesure en aérodynamique*, Les Techniques de l'Ingénieur, R2160, Paris, 1998.

Webographie

[[8]] *http://www.onera.fr/dafe/velocimetrie-laser*